BioSystems 162 (2017) 215–232

Contents lists available at ScienceDirect

BioSystems

journal homepage: www.elsevier.com/locate/biosystems

Review article

Analysis of network motifs in cellular regulation: Structural similarities, input–output relations and signal integration

Ronny Straube

Max Planck Institute for Dynamics of Complex Technical Systems Magdeburg, Sandtorstr. 1, D-39106 Magdeburg, Germany

ARTICLE INFO

Article history:
Received 21 September 2017
Received in revised form 22 October 2017
Accepted 23 October 2017
Available online 28 October 2017

Keywords:
Ultrasensitivity
Substrate competition
Cooperativity
Covalent modification cycles
Two-component systems

ABSTRACT

Much of the complexity of regulatory networks derives from the necessity to integrate multiple signals and to avoid malfunction due to cross-talk or harmful perturbations. Hence, one may expect that the input–output behavior of larger networks is not necessarily more complex than that of smaller network motifs which suggests that both can, under certain conditions, be described by similar equations. In this review, we illustrate this approach by discussing the similarities that exist in the steady state descriptions of a simple bimolecular reaction, covalent modification cycles and bacterial two-component systems. Interestingly, in all three systems fundamental input–output characteristics such as thresholds, ultrasensitivity or concentration robustness are described by structurally similar equations. Depending on the system the meaning of the parameters can differ ranging from protein concentrations and affinity constants to complex parameter combinations which allows for a quantitative understanding of signal integration in these systems. We argue that this approach may also be extended to larger regulatory networks.

Contents

https://doi.org/10.1016/j.biosystems.2017.10.012
0303-2647/

1. Introduction

Biological networks are complex – not just by the number of their components, but also by the number and specificity of their interactions. Despite increasing knowledge of the molecular keyplayers involved in specific regulatory systems and signaling pathways simulating larger networks does not necessarily lead to deeper insights. It has thus become a useful strategy to analyze smaller recurring network structures called network motifs. Since the seminal work of Milo et al. (2002), which originally focused on gene regulatory networks, the systematic analysis of network motifs has led to an increasing list of circuits that may generate specific input–output behavior such as ultrasensitivity and thresholds (Goldbeter and Koshland, 1981; Gunawardena, 2005; Gomez-Uribe et al., 2007), fold-change detection (Geontoro et al., 2009; Adler et al., 2014; Olsman and Geontoro, 2016), concentration robustness (Shinar et al., 2007, 2009; Shinar and Feinberg, 2010) or multistability (Ferrell, 2002; Markevich et al., 2004; Tiwari et al., 2011; Straube and Conradi, 2013). Using methods from control theory network motifs were also analyzed from an engineering perspective (Sauro and Kholodenko, 2004).

Despite this increasing knowledge it has remained challenging to predict the behavior of larger networks based on the known behavior of its constituent parts (Rosenfeld et al., 2007). Exceptions are multistationarity and certain forms of robustness which can be detected based on algebraic properties of a network (Craciun et al., 2006; Conradi et al., 2007; Shinar and Feinberg, 2010; Dexter et al., 2015; Sontag, 2017), i.e. without detailed knowledge of reaction rates and parameters. However, while these methods can be used to decide whether a given system has a certain property they often do not say much about the parameter range or the biological conditions under which a certain behavior occurs. Obtaining this type of information typically requires more detailed analysis of the governing equations which will be the strategy advocated in this review.

To this end, we shall focus on mass-action networks with at most bimolecular interactions. Starting with the most simple of such systems, the receptor–ligand binding motif, we will stepwise extend the analysis to more complex network motifs. First, we show how thresholds and ultrasensitivity can arise through cooperativity in ligand binding and substrate competition. Subsequently, we consider covalent modification cycles which represent the elementary building blocks for many eukaryotic signaling networks such as protein kinase cascades or multisite phosphorylation systems, which are reviewed elsewhere (Heinrich et al., 2002; Salazar and Höfer, 2009; Ferrell and Ha, 2014). Finally, we discuss regulatory properties of two-component systems which share some similarity with covalent modification cycles, but occur mostly in bacteria (Stock et al., 2000). Again, we focus on the most simple regulatory structures leaving out more complicated architectures such as phosphorelay systems (Tiwari et al., 2011).

A major goal of this review is to highlight structural similarities that exist between the steady state equations characterizing the input–output behavior of different network motifs. Despite the fact that the transient dynamics will, in general, be different for different systems it turns out that in certain limiting regimes the steady state behavior of the network motifs considered in this review can be characterized by one of the following three types of (quadratic) equations

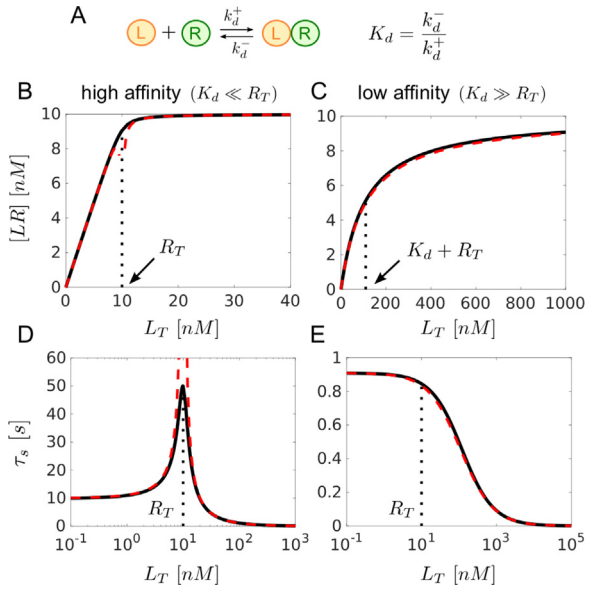

Fig. 1. (A) Receptor–ligand binding motif. (B)–(E) Stimulus-response curves and time scales for reaching a new steady state in the strong and weak binding limits. Solid lines represent the exact solutions in Eq. (7) (B,C) and Eq. (9) (D,E) while the dashed lines denote the approximations in Eq. (10) (B), Eq. (12) (C), Eq. (11) (D) and Eq. (13) (E). Parameters: $k_d^+ = 0.01/(\text{nMs})$, $k_d^- = k_d^+ \cdot K_d$ where $K_d = 0.1$ nM (B,D) and $K_d = 100$ nM (C,E).

$$x^2 - (A + B + C)x + qAB = 0 \tag{1}$$

$$x^2 + (A + B - C)x - BC = 0 \tag{2}$$

$$\alpha \frac{A - x}{B + A - x} = \frac{x}{C + x} \tag{3}$$

where x denotes the concentration for the quantity of interest while A, B, C, q and α denote single parameters or parameter combinations depending on the system. The above three equations arise in the analysis of receptor–ligand binding (Eqs. (1) and (2)) and covalent modification cycles (Eq. (3)) which may, thus, be regarded as 'elementary' network motifs. While the focus of this review lies on small networks and network motifs the presented methods may also be applicable to larger networks.

2. Receptor–ligand binding

2.1. The LR-type equation

The reversible binding of a ligand to a receptor is described by the reaction (Fig. 1A)

$$L + R \underset{k_d^-}{\overset{k_d^+}{\rightleftarrows}} LR$$

where the dissociation constant $K_d = k_d^-/k_d^+$ represents a measure for the binding affinity of the ligand. Assuming that the concentrations of ligand and receptor are contant, i.e.

$$[L] + [LR] = L_T$$
$$[R] + [LR] = R_T \tag{4}$$

the dynamics of the receptor–ligand complex is described by the ordinary differential equation (ODE)

$$\frac{d[LR]}{dt} = k_d^+ (L_T - [LR])(R_T - [LR]) - k_d^- [LR] \tag{5}$$

where L_T and R_T denote the total concentrations of ligand and receptor, respectively. Eq. (5) is one of the few nonlinear equations arising in mathematical biology that is exactly solvable (Tzafriri, 2003). If, initially, the concentration of LR vanishes its solution is given by

$$[LR](t) = [LR]_- \frac{1 - e^{-t/\tau_s}}{1 - ([LR]_-/[LR]_+)e^{-t/\tau_s}} \tag{6}$$

where

$$[LR]_\pm = \frac{L_T + R_T + K_d}{2} \pm \sqrt{\frac{(L_T + R_T + K_d)^2}{4} - L_T R_T} \tag{7}$$

are the solutions of the steady state equation ($d[LR]/dt = 0$)

$$[LR]^2 - (L_T + R_T + K_d)[LR] + L_T R_T = 0, \tag{8}$$

and

$$\tau_s = \frac{1}{k_d^-} \frac{K_d}{\sqrt{(L_T + R_T + K_d)^2 - 4L_T R_T}} \tag{9}$$

denotes the time scale on which the stable steady state is reached for $t \gg \tau_s$ (cf. Eq. (6)). Due to the constraint $0 \le [LR] \le \min(L_T, R_T)$ the latter is given by $[LR]_-$. As shown below the quadratic equation (8) frequently arises in the analysis of network motifs, so we denote it by **LR**-type equation.

It is instructive to analyze the expressions for the steady state and the time scale τ_s in the limits of low and high affinity. For definiteness we consider the receptor concentration as fixed and the ligand concentration as variable. In that case, the high-affinity limit is defined by $K_d \ll R_T$ and the stimulus-response curve can be approximated by (Straube, 2015)

$$[LR] \approx \begin{cases} L_T \left(1 - \dfrac{K_d}{R_T - L_T}\right), & L_T < R_T \\ R_T \left(1 - \dfrac{K_d}{L_T - R_T}\right), & L_T > R_T \end{cases} \tag{10}$$

while the expression for τ_s simplifies to (cf. Section A.1)

$$\tau_s \approx \begin{cases} \dfrac{1}{k_d^-} \dfrac{K_d}{(R_T - L_T)}, & L_T < R_T \\ \dfrac{1}{k_d^-} \dfrac{K_d}{(L_T - R_T)}, & L_T > R_T \end{cases} \tag{11}$$

In the low-affinity limit, defined by $K_d \gg R_T$, the approximations read

$$[LR] \approx \frac{L_T R_T}{K_d + L_T + R_T} \tag{12}$$

$$\tau_s \approx \frac{1}{k_d^-} \frac{K_d}{K_d + L_T + R_T}. \tag{13}$$

Hence, in the high-affinity limit the receptor behaves as a stoichiometric inhibitor since the concentration of the complex increases in 1:1 stoichiometry with the ligand concentration until saturation (Fig. 1B). In contrast, the time scale for reaching the steady state τ_s exhibits a non-monotonic dependence on the ligand concentration with a maximum at $L_T = R_T$ (Fig. 1D). The latter can be rationalized as follows: If there is a surplus of either reaction partner (i.e. $L_T \gg R_T$ or $R_T \gg L_T$) a steady state is quickly reached because the probability for any molecule of the low-abundant species to find a molecule from the high-abundant species is large during the whole course of the reaction in which the high-abundant species is rarely depleted. The situation is different when ligands and receptors are present in comparable amounts (i.e. $L_T \approx R_T$) because in the high-affinity regime essentially all ligands will be bound to receptors in steady state. Hence, as the reaction proceeds both ligand and receptor pools are depleted simultaneously, thereby lowering the reaction rate which increases the time scale for reaching the steady state. In fact, from Eq. (9) one can show that $\tau_s \sim \sqrt{K_d/R_T}$ when $L_T = R_T$ (cf. Section A.1). In contrast, in the low-affinity regime [LR] increases hyperbolically with the ligand concentration while the time scale for reaching the steady state remains almost constant for $L_T < R_T$ and decreases monotonically for $L_T > R_T$ (Fig. 1C and E).

2.2. Synthesis and degradation

It is an interesting question how changing the boundary conditions affects the dynamic behavior of a system. In general, changing boundary conditions may not only affect the transient dynamics, but also the steady state behavior of a system. In the case of receptor–ligand binding Buchler and Louis have shown (Buchler and Louis, 2008) that going from a closed system with mass-conservation to an open system with constitutive synthesis for L and R

$$\emptyset \xrightarrow{k_{s,L}} L,\ \emptyset \xrightarrow{k_{s,R}} R$$

and linear degradation of the form

$$L \xrightarrow{k_{d,L}} \emptyset,\ R \xrightarrow{k_{d,R}} \emptyset,\ LR \xrightarrow{k_{d,LR}} \emptyset$$

leads again to a **LR**-type steady state equation for the receptor–ligand complex that is given by

$$[LR]^2 - \frac{k_{s,L} + k_{s,R} + \kappa}{k_{d,LR}} [LR] + \frac{k_{s,L} k_{s,R}}{k_{d,LR}^2} = 0. \tag{14}$$

Note that Eq. (8) becomes identical with Eq. (14) through the substitution

$$L_T \leftrightarrow \frac{k_{s,L}}{k_{d,LR}},\ R_T \leftrightarrow \frac{k_{s,R}}{k_{d,LR}},\ K_d \leftrightarrow \frac{\kappa}{k_{d,LR}}. \tag{15}$$

Here, $\kappa = \left(k_{d,L} k_{d,R}/k_{d,LR}\right) \kappa_D$ is defined in terms of the *in vivo* dissociation constant $\kappa_D = \left(k_d^- + k_{d,LR}\right)/k_d^+$ which is always larger than the *in vitro* dissociation constant $K_d = k_d^-/k_d^+$. For fixed receptor synthesis rate $k_{s,R}$ one may again define a high-affinity ($\kappa \ll k_{s,R}$) and a low-affinity regime ($\kappa \gg k_{s,R}$), and utilize the correspondence in Eq. (15) to derive approximate expressions similar to those in Eqs. (10) and (12).

2.3. The L-type equation

In many occasions the species of interest is the free form of the ligand rather than the receptor–ligand complex. The steady state equation for the free ligand can be obtained from that of the complex by substituting the conservation relation (4) into Eq. (8) which yields another type of quadratic equation

$$[L]^2 + (R_T + K_d - L_T)[L] - K_d L_T = 0 \tag{16}$$

that we shall denote by **L**-type equation. Using the approximations for [LR] and the conservation relation (4) one can readily

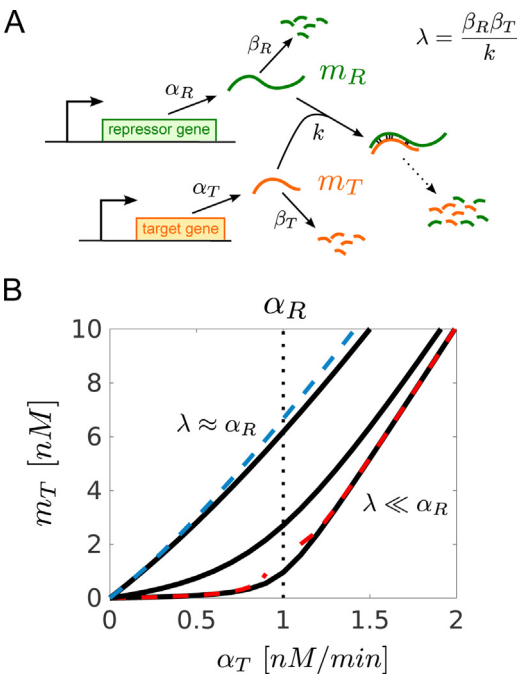

Fig. 2. Tunable threshold in gene regulation. (A) Model for the repression of a target gene through complex formation between target mRNA and repressor mRNA according to (Levine et al., 2007). (B) If the target-repressor interaction is sufficiently strong ($\lambda \ll \alpha_R$) a sharp threshold develops for the onset of target gene expression as a function of the synthesis rate. Solid lines were computed from Eq. (16) with the replacement $([L], L_T, R_T, K_d) \to \left(\beta_T [m_T], \alpha_T, \alpha_R, \lambda\right)$ for $\alpha_R = 1$ nM/s, $\beta_T = 0.1$/min and $\lambda = 0.01, 0.1, 1$ (bottom to top). Red and blue dashed lines were computed from Eqs. (17) and (18), respectively. (For interpretation of the references to color in this figure legend, the reader is referred to the web version of this article.)

derive corresponding approximations for $[L]$. In the high-affinity limit ($K_d \ll R_T$) this yields

$$[L] \approx \begin{cases} \dfrac{K_d L_T}{R_T - L_T}, & L_T < R_T \\ L_T - R_T + \dfrac{K_d R_T}{L_T - R_T}, & L_T > R_T \end{cases} \tag{17}$$

while the low-affinity approximation ($K_d \gg R_T$) becomes

$$[L] \approx L_T \frac{K_d + L_T}{K_d + L_T + R_T} \approx L_T. \tag{18}$$

From the expression in Eq. (17) we see that $[L]$ exhibits threshold behavior, i.e. below the threshold $L_T = R_T$ it remains low ($\mathcal{O}\left(K_d/R_T\right)$), and it increases linearly beyond the threshold.

This threshold-linear response behavior has been observed in diverse systems. It occurs, for example, in the context of molecular titration if the active form of a transcription factor is sequestered by a repressor into an inactive complex (Buchler and Louis, 2008) or if the translation of a mRNA is inhibited through sequestration of the target mRNA by a small repressor RNA (Levine et al., 2007). In the latter case Levine et al. derived the following steady state equation (Fig. 2A)

$$[m_T]^2 + (\alpha_R + \lambda - \alpha_T)\frac{[m_T]}{\beta_T} - \frac{\alpha_T \lambda}{\beta_T^2} = 0, \lambda = \frac{\beta_R \beta_T}{k} \tag{19}$$

which is structurally identical with the **L**-type equation (Eq. (16)). Here, α_R and α_T denote the synthesis rates for repressor and target mRNA whereas $\lambda = \beta_R \beta_T / k$ is related to the mRNA turnover rates and the association rate (Fig. 2A). Similar as for the case of receptor–ligand binding in the 'high-affinity' regime $\lambda \ll \alpha_R$ the concentration of the target mRNA $[m_T]$ remains low until a threshold is crossed beyond which the mRNA level increases proportionally to the synthesis rate (Fig. 2B).

2.4. Approximation at the threshold

In the high-affinity regime the approximations listed in Eqs. (10), (11) and (17) become singular at the threshold ($L_T = R_T$) because the leading order of the exact solution of the quadratic equation becomes of $\mathcal{O}\left(\sqrt{\varepsilon}\right)$ (rather than $\mathcal{O}(\varepsilon)$) where $\varepsilon = K_d/R_T \ll 1$. To see this more explicitly we set $L_T = R_T$ in Eq. (8) and expand its solution as

$$\begin{aligned} [LR] &= R_T + \frac{K_d}{2} - \sqrt{K_d R_T + \frac{K_d^2}{4}} \\ &= R_T \left(1 - \sqrt{\varepsilon} + \mathcal{O}(\varepsilon)\right). \end{aligned}$$

To reproduce this solution to leading order we modify the approximation in Eq. (10) as (cf. Levine et al., 2007)

$$[LR] \approx \begin{cases} L_T \left(1 - \dfrac{K_d}{R_T - L_T + \sqrt{K_d R_T}}\right), & L_T \le R_T \\ R_T \left(1 - \dfrac{K_d}{L_T - R_T + \sqrt{K_d R_T}}\right), & L_T \ge R_T \end{cases} \tag{20}$$

Using the same procedure one may derive improved approximations for τ_s (Eq. (11)) and $[L]$ (Eq. (17)) as well as for many of the approximations given in the remainder of this review.

2.5. Independent binding to a scaffold protein

Signal transduction often involves recruitment of signaling molecules to a scaffold protein (Witzel et al., 2012) which one may think of as kinases for definiteness (Fig. 3A). If binding of each kinase to the scaffold occurs independently the probability for the occurrence of a fully assembled complex consisting of the scaffold and n kinases is given by

$$p_n(SK_1 \ldots K_n) = \prod_{i=1}^{n} p_1(SK_i)$$

where $p_1(SK_i) = [SK_i]/S_T$ is the probability for binding of a single kinase to the scaffold. In that case the concentration of the fully assembled complex can be computed from (cf. (Borisov et al., 2005))

$$[SK_1 \ldots K_n] = \frac{\prod_{i=1}^{n} [SK_i]}{S_T^{n-1}} \tag{21}$$

where the concentration of a single scaffold-kinase complex is determined by the **LR**-type equation (cf. Eq. (8))

$$[SK_i]^2 - [SK_i](S_T + K_{iT} + K_{di}) + S_T K_{iT} = 0. \tag{22}$$

Here, S_T denotes the total concentration of the scaffold while K_{iT} and K_{di} denote the total concentrations of the kinases and their dissociation constants, respectively.

The approximate expressions derived for the solution of Eq. (22) can now be used to construct explicit expressions for the concentration of the fully assembled complex. To illustrate this procedure we consider the case $n = 3$. If all three kinases are of high affinity

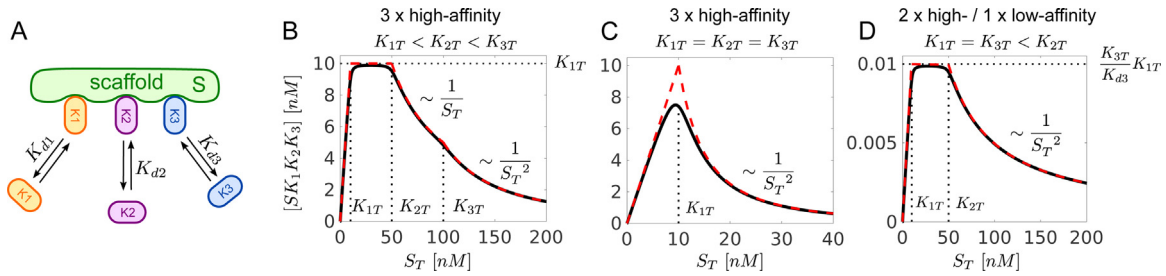

Fig. 3. Ligand binding to a scaffold protein may lead to concentration robustness. (A) Three kinases (K1–K3) bind independently to a scaffold S with dissociation constants K_{di}. (B–D) Stimulus-response curves for the fully assembled complex as a function of the scaffold concentration. If at least two high-affinity kinases bind to the scaffold a plateau regime exists in the region $K_{1T} < S_T < K_{2T}$ where the concentration of the fully assembled complex does not depend on the scaffold concentration. Parameters: (B) $K_{1T} = 10$ nM, $K_{2T} = 50$ nM, $K_{3T} = 100$ nM, $K_{di} = 0.1$ nM. (C) $K_{iT} = 10$ nM, $K_{di} = 0.1$ nM. (D) $K_{1T} = K_{3T} = 10$ nM, $K_{2T} = 50$ nM, $K_{d1} = K_{d2} = 0.1$ nM, $K_{d3} = 10^4$ nM.

(so that $K_{di} \ll K_{iT}$ for $i = 1, 2, 3$) the stimulus-response curve for the fully assembled complex can be approximated by (cf. Fig. 3B)

$$[SK_1K_2K_3] \approx \begin{cases} S_T, & 0 < S_T < K_{1T} \\ K_{1T}, & K_{1T} < S_T < K_{2T} \\ \dfrac{K_{1T}K_{2T}}{S_T}, & K_{2T} < S_T < K_{3T} \\ \dfrac{K_{1T}K_{2T}K_{3T}}{S_T^2}, & K_{3T} < S_T \end{cases} \tag{23}$$

Here, we have assumed without loss of generality that $K_{1T} < K_{2T} < K_{3T}$. Interestingly, in the regime $K_{1T} < S_T < K_{2T}$ the concentration of the fully assembled complex is independent of the scaffold concentration, i.e. the system exhibits 'concentration robustness' with respect to changes in S_T in that regime. The extent of this regime can be tuned by changing the concentrations of the two least abundant kinases (Witzel et al., 2012). Indeed, when the concentrations of all kinases become equal the two middle regimes in Eq. (23) disappear leaving a sharp maximum at $S_T = K_{iT}$ in the response curve (Fig. 3C). As demonstrated in Fig. 3D a plateau can also be generated with two high-affinity kinases (K_1 and K_2) and one low-affinity kinase (K_3). Combining the corresponding expressions for the high- and low-affinity approximations of Eq. (22) yields

$$[SK_1K_2K_3] \approx \frac{K_{3T}}{K_{3T} + S_T + K_{d3}} [SK_1K_2]$$

where $[SK_1K_2]$ is given by

$$[SK_1K_2] \approx \begin{cases} S_T, & 0 < S_T < K_{1T} \\ K_{1T}, & K_{1T} < S_T < K_{2T} \\ \dfrac{K_{1T}K_{2T}}{S_T}, & K_{2T} < S_T \end{cases} \tag{24}$$

However, since $K_{3T} \ll K_{d3}$ for the low-affinity kinase the activity of the fully assembled complex in the plateau regime is substantially reduced by a factor $K_{3T}/K_{d3} \ll 1$ compared to the case of three high-affinity kinases (Eq. (23)).

2.6. Cooperativity and molecular exchange systems

If binding of one ligand affects binding of another ligand the system is said to exhibit cooperativity. The analysis of such a scenario is more complicated and even in the simplest case of two ligands (Fig. 4A) no general solution exists. Depending on whether binding of the first ligand favors or hinders binding of the next one the cooperativity can be positive or negative, respectively. The cooperative-binding motif arises in many different contexts. Classically, it described mixed-type inhibition of an enzyme-catalyzed reaction (Cornish-Bowden, 2004) where S, K_1 and K_2 correspond to the enzyme, the substrate and the inhibitor, respectively. The same pattern was also used in a pharmacological context to estimate the binding affinities of drugs that interact allosterically with a receptor (Ehlert, 1988). Recently, this motif has been studied in the context of two-component signaling where a signaling molecule controls the interaction between a modulator and a response regulator (Babel and Bischofs, 2016).

The steady states of the cooperative-binding motif are described by 3 of the 4 binding equilibria, e.g.

$$\begin{aligned} [S][K_1] &= K_{d1}[SK_1] \\ [SK_1][K_2] &= K_{d2}^*[SK_1K_2] \\ [SK_2][K_1] &= K_{d1}^*[SK_1K_2] \end{aligned} \tag{25}$$

together with the three conservation relations

$$\begin{aligned} [S] + [SK_1] + [SK_2] + [SK_1K_2] &= S_T \\ [K_1] + [SK_1] + [SK_1K_2] &= K_{1T} \\ [K_2] + [SK_2] + [SK_1K_2] &= K_{2T}. \end{aligned} \tag{26}$$

Since the free energy change for the formation of the ternary complex (SK_1K_2) must not depend on the order in which it was formed the 4th dissociation constant K_{d2} is determined by the other three constants through the detailed balance relation

$$K_{d1} \cdot K_{d2}^* = K_{d2} \cdot K_{d1}^*.$$

To characterize the steady state operating regimes of the cooperative-binding motif it is useful to introduce two parameters that measure cooperativity (c) and bias (b) as

$$c = \frac{K_{d2}}{K_{d1}^*}, \; b = \frac{K_{d2}}{K_{d1}} = \frac{K_{d2}^*}{K_{d1}^*}.$$

Similar as in the case of the receptor–ligand binding motif one may distinguish a high-affinity and a low-affinity regime (cf. Fig. 1). Together with the limiting regimes of strong positive ($c \gg 1$) or strong negative ($c \ll 1$) cooperativity and strong bias ($b \ll 1$) or no bias ($b = 1$) there are potentially 8 interesting operating regimes for this motif.

Recently, Ha et al. showed that in the high-affinity regime ($K_{d1}^* \ll S_T$) the steady states of the ternary complex $[SK_1K_2]$, defined by Eqs. (25) and (26), can be approximated by the set $\mathcal{S} = \{S_T, K_{1T}, K_{2T}, x_+, x_-\}$ where $x_\pm$ are the roots of the quadratic equation (Ha et al., 2016)

$$x^2 - \left(K_{1T} + K_{2T} + \frac{b}{c-b} S_T\right) x + \frac{c}{c-b} K_{1T}K_{2T} \approx 0. \tag{27}$$

This equation can be viewed as a **generalized LR**-type equation where the constant term involves the additional scaling factor $c/(c-b)$ (cf. Eq. (1)). The elements in $\mathcal{S}$ can be combined to yield approximate expressions for the stimulus-response curve as a

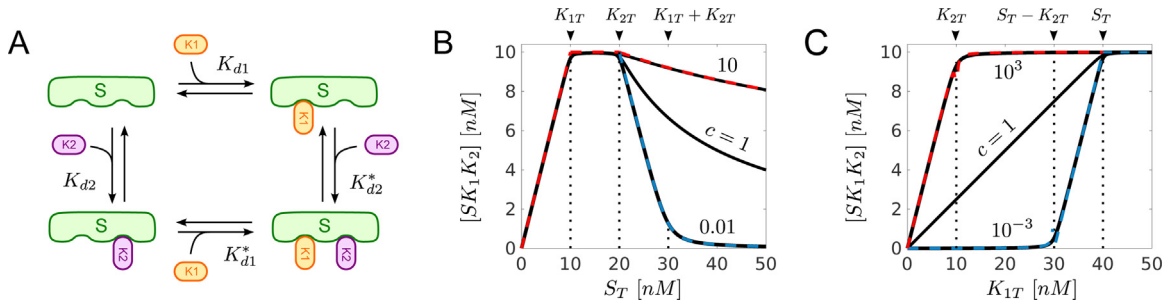

Fig. 4. Cooperativity between ligands binding to a scaffold. (A) Two kinases bind to a scaffold such that $c = K_{d2}/K^*_{d1} > 1$ (positive cooperativity) or $c < 1$ (negative cooperativity). (B) Negative cooperativity leads to more localized concentration profiles for $[SK_1K_2]$ as a function of the scaffold concentration ($K_{1T} = 10$ nM, $K_{2T} = 20$ nM). (C) Strong negative cooperativity generates a sharp threshold and ultrasensitivity for $[SK_1K_2]$ as a function of the kinase concentration ($S_T = 40$ nM, $K_{2T} = 10$ nM). Note that stimulus-response curves are partially overlapping for $S_T \le K_{2T}$ (B) and $K_{1T} \ge S_T$ (C). Dashed lines were computed according to Eqs. (28) (B) as well as Eq. (31) (C, red curve) and Eq. (32) (C, blue curve). Other parameters: $b = 1$, $K^*_{d1} = 0.01nM$. (For interpretation of the references to color in this figure legend, the reader is referred to the web version of this article.)

function of various parameters. For example, if $K_{1T} < K_{2T}$ the concentration of SK_1K_2 as a function of S_T is given by

$$[SK_1K_2] \approx \begin{cases} S_T, & 0 < S_T < K_{1T} \\ K_{1T} & K_{1T} < S_T < K_{2T} \\ x_{\pm}, & K_{2T} < S_T \end{cases} \tag{28}$$

where $x_{\pm}$ denote the positive (x_+) or negative (x_-) square root solution of Eq. (27) depending on whether $c < b$ or $c > b$, respectively (Fig. 4B). If $c = b$ Eq. (27) has just the single solution $x = K_{1T}K_{2T}/S_T$ which declines to zero as $1/S_T$, similarly as in the case of independent binding (cf. Eq. (24)). In the case of strong positive cooperativity ($c \gg b$) the asymptotic decline of $[SK_1K_2]$ is described by (cf. Section A.2)

$$x_- \sim \frac{K_{1T}K_{2T}}{K_{1T} + K_{2T} + \varepsilon S_T}, S_T \gg \frac{K_{1T} + K_{2T}}{\varepsilon} \tag{29}$$

where $\varepsilon \equiv b/(c-b) \ll 1$, i.e. the concentration of the ternary complex decays more slowly as in the case of independent binding (Fig. 4B). In contrast, for strong negative cooperativity ($c \ll b$) the solution of Eq. (27) can be approximated by

$$x_+ \approx \begin{cases} K_{1T} + K_{2T} - S_T, & K_{2T} \le S_T < K_{1T} + K_{2T} \\ \eta \dfrac{K_{1T}K_{2T}}{S_T - (K_{1T} + K_{2T})}, & S_T > K_{1T} + K_{2T} \end{cases} \tag{30}$$

where $\eta \equiv c/(b-c) \ll 1$, i.e. in the regime $K_{2T} \le S_T < K_{1T} + K_{2T}$ the concentration of the ternary complex decreases almost linearly leading to a more "localized" concentration profile.

Alternatively, when considered as a function of the kinase concentration K_{1T} under conditions when the scaffold is not saturated ($S_T > K_{2T}$) strong positive cooperativity generates a stimulus-response curve

$$[SK_1K_2] \approx \begin{cases} K_{1T}(1 - \varepsilon \dfrac{S_T - K_{2T}}{K_{2T} - K_{1T}}), & 0 \le K_{1T} < K_{2T} \\ K_{2T}(1 - \varepsilon \dfrac{S_T - K_{1T}}{K_{1T} - K_{2T}}), & K_{\{2T\}} \le K_{\{1T\}} < S_T \\ K_{2T}, & S_T \le K_{1T} \end{cases} \tag{31}$$

which is of linear-saturation shape (Fig. 4C, red curve) similar as obtained for receptor–ligand binding in the case of a high-affinity ligand (Fig. 1B). In the limit of strong negative cooperativity the approximation for the stimulus-response curve reads

$$[SK_1K_2] \approx \begin{cases} \eta \dfrac{K_{1T}K_{2T}}{(S_T - K_{2T}) - K_{1T}}, & 0 \le K_{1T} < S_T - K_{2T} \\ K_{1T} - (S_T - K_{2T}), & S_T - K_{\{2T\}} < K_{\{1T\}} < S_T \\ K_{2T}, & S_T \le K_{1T} \end{cases} \tag{32}$$

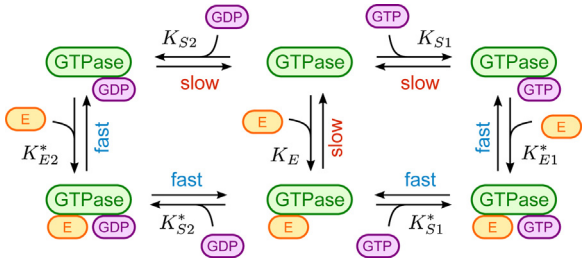

Fig. 5. Molecular exchange system operate under conditions of strong negative cooperativity ($K^*_{Si} \gg K_{Si}$, $i = 1,2$). Binding of the exchange factor E to the GTPase lowers the binding affinities for GTP and GDP from the ternary complexes. In the presence of a high GTP/GDP ratio E mediates the exchange of GDP for GTP favoring the formation of the GTP.GTPase state.

which shows that in the transition region, defined by $S_T - K_{2T} < K_{1T} \le S_T$, the response curve changes in an ultrasensitive manner from $\mathcal{O}(\eta)$ to K_{2T} (Fig. 4C, blue curve). The width of the transition region as well as the maximal amplitude of the response are given by K_{2T}, i.e. steep responses require $K_{2T} \ll S_T$ which limits the dynamic range of the output. By combining theory with experiments Ha and Ferrell recently showed that negative cooperativity may lead to sharp thresholds and ultrasensitivity in the cooperative binding motif for the case of two identical ligands (Ha and Ferrell, 2016).

Another class of systems that operates under conditions of strong negative cooperativity are molecular exchange systems (Fig. 5). A prominent example are small GTPases which alter between an inactive GDP-bound form and a GTP-bound form that can act as a signaling molecule for a large variety of cellular processes (Cherfils and Zeghouf, 2013). In isolation the binary GTPase.GDP/GTPase.GTP complexes are extremely stable with half-lifes between hours and days (Goody and Hofmann-Goody, 2002). However, in the presence of a guanine nucleotide exchange factor (GEF) the dissociation constants of GDP and GTP from the GTPase are increased by several orders of magnitude leading to their rapid dissociation and to nucleotide exchange (Fig. 5). Mathematical models have shown that there exist intrinsic trade-offs in molecular exchange systems (Goryachev and Pokhilko, 2006; Straube et al., 2017) which, in the case of the GTPase cycle, predict an optimal concentration for the GEF as a result of a trade-off between high GTPase activity and fast GDP/GTP cycling.

2.7. Substrate competition and thresholds

Substrate competition arises if at least two ligands compete for a single binding site on a receptor (Fig. 6A). Examples of substrate competition are numerous including gene regulation by small RNAs

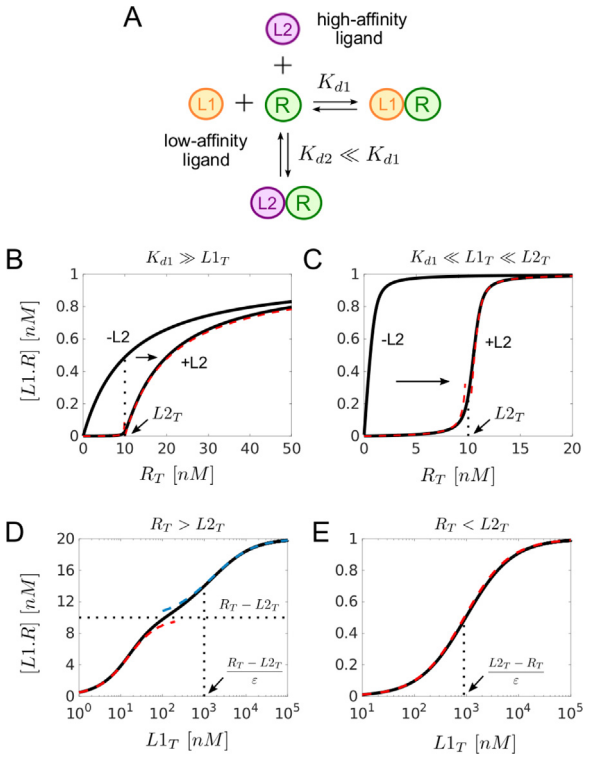

Fig. 6. Generation of a threshold and ultrasensitivity through substrate competition. (A) Two ligands (L1 and L2) compete for binding to a receptor (R). (B,C) Steady state concentration of the ligand–receptor complex as a function of receptor concentration for $K_{d1} = 10$ nM, $K_{d2} = 0.01$ nM (B) and $K_{d1} = 0.1$ nM, $K_{d2} = 0.001$ nM (C) so that $\varepsilon = K_{d2}/K_{d1} \ll 1$. ±L2 indicate the presence (+) or absence (−) of L2 ($L2_T = 0$). Other parameters: $L1_T = 1$ nM, $L2_T = 10$ nM. Red dashed lines were drawn according to Eqs. (37) and (38). (D,E) $[L1.R]$ as a function of the concentration of the low-affinity ligand for $R_T = 20$ nM (D) and $R_T = 1$ nM (E). Other parameters: $L2_T = 10$ nM, $K_{d1} = 10$ nM, $K_{d2} = 0.1$ nM. Blue dashed curve was drawn from Eq. (40) while red dashed lines correspond to Eqs. (38) (D) and (41) (E). (For interpretation of the references to color in this figure legend, the reader is referred to the web version of this article.)

(Levine et al., 2007; Mukherji et al., 2011) and during development (Kim et al., 2010, 2011), binding of substrate receptors to ubiquitin E3 ligases (Petroski and Deshaies, 2005; Lydeard et al., 2013), phosphorylation/dephosphorylation cycles (Kim and Ferrell, 2007; Rowland et al., 2012) and bacterial two-component systems (Laub and Goulian, 2007; Rowland and Deeds, 2014), the latter two being discussed in Sections 3.3 and 4.3, respectively.

Here, we consider the simplest form of substrate competition as it arises when two ligands bind to a scaffold protein or to a receptor (Fig. 6A). In that case the steady states are determined by the two binding equilibria

$$K_{d1}\,[L1.R] = [L1]\,[R]\,,\; K_{d2}\,[L2.R] = [L2]\,[R] \tag{33}$$

and the three conservation relations

$$\begin{aligned} [L1] + [L1.R] &= L1_T \\ [L2] + [L2.R] &= L2_T \\ [R] + [L1.R] + [L2.R] &= R_T. \end{aligned} \tag{34}$$

Combining Eqs. (33) and (34) yields a cubic polynomial which can be written in the form (Straube, 2015)

$$(1-\varepsilon)[L1.R]^3 - a_2[L1.R]^2 - a_1\,[L1.R] + \varepsilon R_T L1_T^2 = 0 \tag{35}$$

where a_2 and a_1 are given by

$$\begin{aligned} a_2 &= -(L1_T + R_T - L2_T + K_{d1}) + \varepsilon\,(2L1_T + R_T + K_{d1}) \\ a_1 &= L1_T\,(R_T - L2_T) - \varepsilon L1_T\,(L1_T + 2R_T + K_{d1})\,. \end{aligned}$$

Depending on the value of $\varepsilon = K_{d2}/K_{d1}$ some interesting limiting regimes can be considered.

2.7.1. Competition by relative abundance

If both ligands exhibit the same affinity ($K_{d1} = K_{d2} \equiv K_d$), so that competition only arises through relative ligand abundances, the cubic polynomial reduces to a **LR**-type equation

$$[L1.R]^2 - [L1.R]\,(L1_T + \rho R_T + \rho K_d) + \rho R_T L1_T = 0,$$

i.e. compared to Eq. (8) the receptor concentration R_T and the dissociation constant K_d are rescaled by a factor

$$\rho = \frac{L1_T}{L1_T + L2_T}$$

which measures the relative abundance of L1. From the expressions in Eqs. (10) and (12) one may readily obtain the corresponding approximations in the high-affinity ($K_d \ll R_T$) and low-affinity regimes ($K_d \gg R_T$) as

$$[L1.R] \approx \begin{cases} L1_T, & L1_T < R_T - L2_T \\ \dfrac{L1_T}{L1_T + L2_T} R_T, & L1_T > R_T - L2_T \end{cases} \tag{36}$$

and

$$[L1.R] \approx \frac{(L1_T + L2_T)\,R_T}{L1_T + L2_T + R_T + K_d}$$

respectively. Hence, under conditions when the receptor is saturated ($L1_T + L2_T > R_T$) the receptor–ligand complex for high-affinity ligands (Eq. (36)) increases proportional to the relative abundance of a ligand – in agreement with intuition.

2.7.2. Strong substrate competition

If the affinity of one ligand is much higher than that of the other one the solutions of the cubic equation (Eq. (35)) can be analyzed in the limit of strong substrate competition $\varepsilon \ll 1$ which may lead to thresholds and ultrasensitivity (Straube, 2015). For receptor concentrations below the threshold (which occurs at $R_T = L2_T$) the concentration of $L1$. R remains low

$$[L1.R] \approx \varepsilon \frac{L1_T R_T}{L2_T - R_T},\; R_T < L2_T \tag{37}$$

since $L2$ sequesters all receptors away. Beyond the threshold ($R_T > L2_T$) the response curve can, again, be approximated by the solution of a **LR**-type equation

$$[L1.R]^2 - [L1.R]\left(L1_T + R_T^{eff} + K_{d1}\right) + L1_T R_T^{eff} \approx 0 \tag{38}$$

where $R_T^{\text{eff}} = R_T - L2_T$ denotes the effective receptor concentration. The latter accounts for the fact that the low-affinity ligand can only bind to receptor molecules that are not yet bound by high-affinity ligands.

Depending on the relative magnitude between K_{d1} and $L1_T$ one may use similar approximations for the solutions of Eq. (38) as for the single ligand in Eqs. (10) and (12). Hence, if $K_{d1} \gg L1_T$ the response curve increases hyperbolically beyond the threshold (Fig. 6B) while for $K_{d1} \ll L1_T$ the response curve may become highly ultrasensitive (Fig. 6C). In the latter regime one obtains the approximation

$$[L1.R] \approx \begin{cases} \varepsilon \dfrac{L1_T R_T}{L2_T - R_T}, & 0 \le R_T < L2_T \\ R_T - L2_T, & L2_T < R_T < L1_T + L2_T \\ L1_T, & L1_T + L2_T \le R_T \end{cases} \tag{39}$$

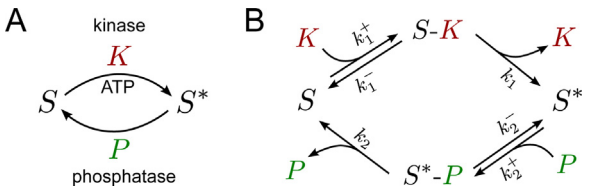

Fig. 7. Covalent modification cycle: (A) The substrate S is phosphorylated by a kinase (K) with ATP as a cofactor and dephosphorylated by a phosphatase (P). (B) Detailed reaction scheme assuming both kinase and phosphatase reaction follow a Michaelis–Menten scheme and the ATP concentration is constant.

Comparing this stimulus-response curve with that for negative cooperativity (Eq. (32)) we see that both exhibit a tripartite structure with a linear increase in the middle regime. In particular, there exists a similar trade-off between the steepness of the response curve, which decreases with $L1_T$, and the dynamic range, which increases with $L1_T$.

The response curve for $[L1.R]$ as a function of the ligand concentration $L1_T$ can exhibit biphasic behavior and is, thus, more difficult to obtain (cf. Section A.3). Note that the asymptotic value for $[L1.R]$ in the limit of $L1_T \gg K_{d1}$, as predicted by Eq. (38), is R_T^{eff} rather than R_T. Hence, the latter describes the relation between $[L1.R]$ and $L1_T$ only at sufficiently low ligand concentrations. A more detailed analysis of the cubic equation (Eq. (35)) shows that the behavior of $[L1.R]$ for large $L1_T$ can be approximated by the solution of the **L**-type equation (Fig. 6D) (cf. Section A.3)

$$[L1.R]^2 + [L1.R](L2_T + \varepsilon L1_T - R_T) - \varepsilon L1_T R_T = 0. \tag{40}$$

When $R_T < L2_T$ one may obtain an approximate solution of this equation by balancing the linear and the constant term

$$[L1.R] \approx \frac{L1_T R_T}{L1_T + \frac{L2_T - R_T}{\varepsilon}}, R_T < L2_T. \tag{41}$$

In that case the approximation is valid for all ligand concentrations and the stimulus-response curve exhibits no biphasic behavior (Fig. 6E).

3. Covalent modification cycles

3.1. Goldbeter–Koshland model and the GK-type equation

In 1981 Goldbeter and Koshland proposed a simple mechanism through which biological systems can generate extremely high sensitivity (known as zero-order ultrasensitivity) to input signals (Goldbeter and Koshland, 1981). Interestingly, the mechanism did not involve cooperative binding of ligands to an oligomeric enzyme rather than two (converter) enzymes catalyzing the covalent modification and demodification of a target protein by utilizing energy in the form of ATP. Often, such futile cycles occur in the form of phosphorylation / dephosphorylation cycles as mediated by a kinase and a phosphatase, respectively (Fig. 7), but energy in the form of ATP is also required for other covalent modifications such as ubiquitylation or neddylation (Dye and Schulman, 2007).

The dynamics of phosphorylation/dephosphorylation cycles, as described by Fig. 7B, is determined by the ODE system

$$\frac{d[S^*]}{dt} = k_1[SK] - k_2^+[S^*][P] + k_2^-[S^*P] \tag{42}$$

$$\begin{aligned} \frac{d[SK]}{dt} &= k_1^+[S][K] - \left(k_1^- + k_1\right)[SK] \\ \frac{d[S^*P]}{dt} &= k_2^+[S^*][P] - \left(k_2^- + k_2\right)[S^*P] \end{aligned} \tag{43}$$

where $[S]$, $[K]$ and $[P]$ have to be replaced using the conservation relations

$$[S] + [S^*] + [SK] + [S^*P] = S_T$$

$$[K] + [SK] = K_T$$

$$[P] + [S^*P] = P_T.$$

The Goldbeter–Koshland model is based on two assumptions: (i) the enzyme-substrate complexes rapidly approach a quasi-stationary state defined by

$$\frac{d[SK]}{dt} \approx \frac{d[S^*P]}{dt} \approx 0,$$

and the substrate concentration is much higher than that of the converter enzymes, i.e.

$$S_T \gg \max(K_T, P_T),$$

which allows simplifying the conservation relation for the substrate as $[S] + [S^*] \approx S_T$. Under these conditions Goldbeter and Koshland derived the following ODE for the concentration of S^* (Goldbeter and Koshland, 1981)

$$\frac{d[S^*]}{dt} \approx k_1 K_T \frac{S_T - [S^*]}{K_1 + S_T - [S^*]} - k_2 P_T \frac{[S^*]}{K_2 + [S^*]}. \tag{44}$$

Here, K_T, P_T and S_T denote the total concentrations of kinase, phosphatase and substrate while $K_i = (k_i + k_i^-)/k_i^+$ are the corresponding Michaelis–Menten constants. The steady state equation $(d[S^*]/dt = 0)$ derived from Eq. (44) will be denoted as **GK**-type equation. Note that it is structurally similar to Eq. (3) mentioned in the Introduction.

To characterize the steady state operating regimes of covalent modification cycles it is useful to introduce dimensionless quantities through $x = [S^*]/S_T$ and $K_i^* = K_i/S_T$ which yields the steady state equation

$$x^2 - \left(1 + \frac{K_1^* + \alpha K_2^*}{1 - \alpha}\right)x + \frac{\alpha K_2^*}{1 - \alpha} = 0, \alpha = \frac{k_1 K_T}{k_2 P_T} \tag{45}$$

where α is the ratio between the maximal rates of kinase and phosphatase. The solution of Eq. (45) reads

$$x = \begin{cases} x_-, & \alpha < 1 \\ x_+, & \alpha > 1 \end{cases} \tag{46}$$

where $x_\pm$ are given by

$$x_\pm = \frac{1}{2}\left(1 + \frac{K_1^* + \alpha K_2^*}{1 - \alpha}\right) \pm \frac{1}{2}\sqrt{\left(1 + \frac{K_1^* + \alpha K_2^*}{1 - \alpha}\right)^2 - 4\frac{\alpha K_2^*}{1 - \alpha}}.$$

A systematic analysis of the steady state operating regimes of covalent modification cycles was given by Gomez-Uribe et al. (2007). Depending on whether the converter enzymes are saturated ($K_i^* \ll 1$) or unsaturated ($K_i^* \gg 1$) there exist 4 operating regimes as depicted in Fig. 8. Zero-order ultrasensitivity requires both enzymes to be saturated ($\max\left(K_1^*, K_2^*\right) \ll 1$). On the other hand if both enzymes are unsaturated ($\min\left(K_1^*, K_2^*\right) \gg 1$) the response curve resembles that of a Michaelian enzyme (Fig. 8B).

Interestingly, if the two converter enzymes operate in opposite regimes the steady state equation resulting from Eq. (44) becomes similar to one of the two quadratic equations shown in Eqs. (1) and (2). Specifically, if the phosphatase is saturated while the kinase is unsaturated ($K_2^* \ll 1 \ll K_1^*$) linearization of the first term in Eq. (44) results in the **L**-type equation

$$x^2 + \left(\frac{K_1^*}{\alpha} + K_2^* - 1\right)x - K_2^* \approx 0. \tag{47}$$

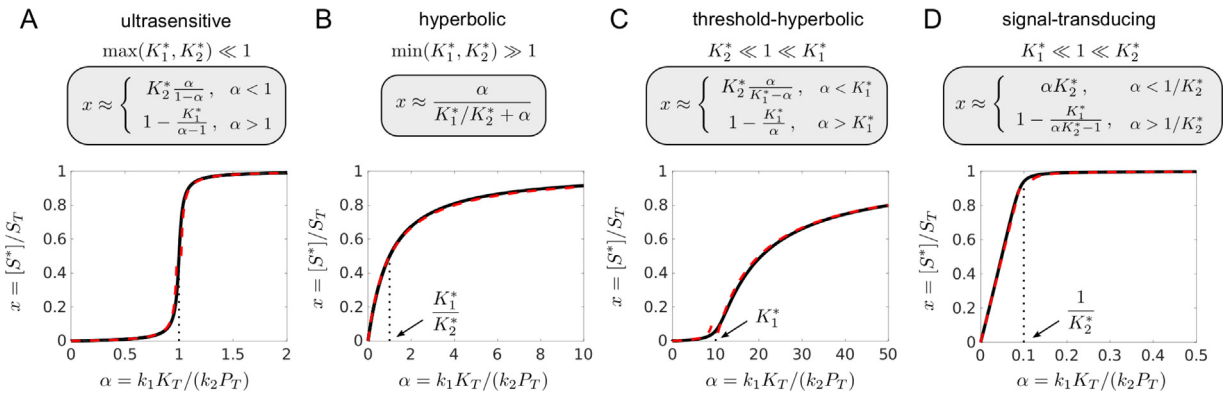

Fig. 8. Steady state operating regimes of covalent modification cycles within the Goldbeter–Koshland model. Solid lines were computed from Eq. (46). Red dashed lines correspond to the approximate expressions shown above each panel. Parameters: (A) $K_1^* = K_2^* = 0.01$, (B) $K_1^* = K_2^* = 10$, (C) $K_1^* = 10$, $K_2^* = 0.01$, (D) $K_1^* = 0.01$, $K_2^* = 10$. (For interpretation of the references to color in this figure legend, the reader is referred to the web version of this article.)

Since, by assumption, $K_2^* \ll 1$ the response curve exhibits a threshold defined by $K_1^*/\alpha = 1$ beyond which the response curve increases hyperbolically as a function of α (Fig. 8C). In the opposite case ($K_1^* \ll 1 \ll K_2^*$) linearization of the second term in Eq. (44) results in the **LR**-type equation

$$x^2 - \left(\alpha K_2^* + K_1^* + 1\right) x + \alpha K_2^* \approx 0. \tag{48}$$

Since, by assumption, $K_1^* \ll 1$ the response curve is of linear-saturation type (Fig. 8D) similar to that of the receptor–ligand complex in the limit of a high-affinity ligand (Fig. 1B). In this case the saturation threshold is defined by $\alpha K_2^* = 1$.

3.2. High enzyme concentrations

One of the limitations of the Goldbeter–Koshland model is that it only applies if the substrate concentration is much higher than that of the converter enzymes. While this condition is routinely used for *in vitro* experiments it is rarely satisfied *in vivo* (Blüthgen et al., 2006; Legewie et al., 2008). To analyze enzyme-catalyzed reactions at high enzyme concentrations Borghans et al. proposed a simple method, known as the total quasi-steady state approximation (tQSSA), involving a linear change of variables (Borghans et al., 1996). Their original motivation was to extend the parameter domain for the applicability of the standard QSSA (Segel and Slemrod, 1989). Later on, the conditions for the validity of the tQSSA have been refined (Schnell and Maini, 2000; Tzafriri, 2003), and the method has been successfully applied to more complicated reaction systems such as the reversible Michaelis–Menten reaction (Tzafriri and Edelman, 2004), substrate competition (Pedersen et al., 2007), covalent modification cycles (Gomez-Uribe et al., 2007; Ciliberto et al., 2007; Pedersen et al., 2010) and to describe the transient phase kinetics (Masia et al., 2016).

The tQSSA is based on the idea to introduce the total concentration of the phosphorylated substrate as a slow variable

$$[Y^*] = [S^*] + [S^*P].$$

Then, addition of Eqs. (42) and (43) leads to

$$\frac{d[Y^*]}{dt} = k_1 [SK] - k_2 [S^*P]. \tag{49}$$

Here, the concentrations of the enzyme-substrate complexes are determined by **LR**-type equations of the form

$$[SK]^2 - (K_T + S_T - [Y^*] + K_1)[SK] + K_T (S_T - [Y^*]) = 0 \tag{50}$$

$$[S^*P]^2 - (P_T + [Y^*] + K_2)[S^*P] + P_T [Y^*] = 0. \tag{51}$$

Substituting the positive solutions of Eqs. (50) and (51) into Eq. (49) yields the total QSSA. Compared to the standard QSSA (Eq. (44)) it more accurately describes the transient dynamics of covalent modification cycles (Ciliberto et al., 2007).

However, the total QSSA can also be used to extend the classification of the steady state operating regimes given by Gomez-Uribe et al. (Fig. 8) to the case when the concentrations of the converter enzymes are comparable to or larger than that of the substrate (Straube, 2017). To this end, we approximate the solutions of Eqs. (50) and (51) in the limit of high ($K_1 \ll K_T$ and $K_2 \ll P_T$) and low affinity ($K_1 \gg K_T$ and $K_2 \gg P_T$). In the first case (low-K_M regime) this yields the approximations

$$[SK] \approx \begin{cases} K_T, & [Y^*] < S_T - K_T \\ S_T - [Y^*], & [Y^*] > S_T - K_T \end{cases} \tag{52}$$

and

$$[S^*P] \approx \begin{cases} [Y^*], & [Y^*] < P_T \\ P_T, & [Y^*] > P_T \end{cases} \tag{53}$$

In the second case (high-K_M regime) the approximations read

$$[SK] \approx \frac{K_T (S_T - [Y^*])}{K_T + S_T - [Y^*] + K_1} \tag{54}$$

$$[S^*P] \approx \frac{P_T [Y^*]}{P_T + [Y^*] + K_2}. \tag{55}$$

Altogether this defines 4 operating regimes depending on the ratio between the Michaelis–Menten constants and the concentrations of the converter enzymes. To derive approximate expressions for $[Y^*]$ in a particular regime one has to combine the expressions in Eqs. (52)–(55) in an appropriate manner. Depending on the parameter of interest and the values of the remaining parameters several subregimes may exist. For example, if both enzymes are saturated ($K_1 \ll K_T$ and $K_2 \ll P_T$) and the total enzyme concentration exceeds that of the substrate ($K_T + P_T > S_T$) there are 4 subregimes defining $[Y^*]$ as a function of k_1 depending on whether $K_T \lessgtr S_T$ and $P_T \lessgtr S_T$ (Fig. 9). Interestingly, when at least one of the enzyme concentrations is lower than that of the substrate the response curve exhibits enhanced sensitivity with $n_H > 1$ (Fig. 9A–C). Conversely, when at least one of the enzyme concentrations is larger than that of the substrate the response curve is independent of that enzyme concentration, i.e. the system exhibits concentration robustness with respect to changes in that particular enzyme concentration. For example, if $K_T > S_T$ the response curve becomes independent of K_T although it still depends on P_T (Fig. 9B). Finally, if both enzyme concentrations exceed that of the substrate the response curve only depends on the catalytic rate constants and the substrate concentration (Fig. 9D). Together, this suggests that there are two regimes

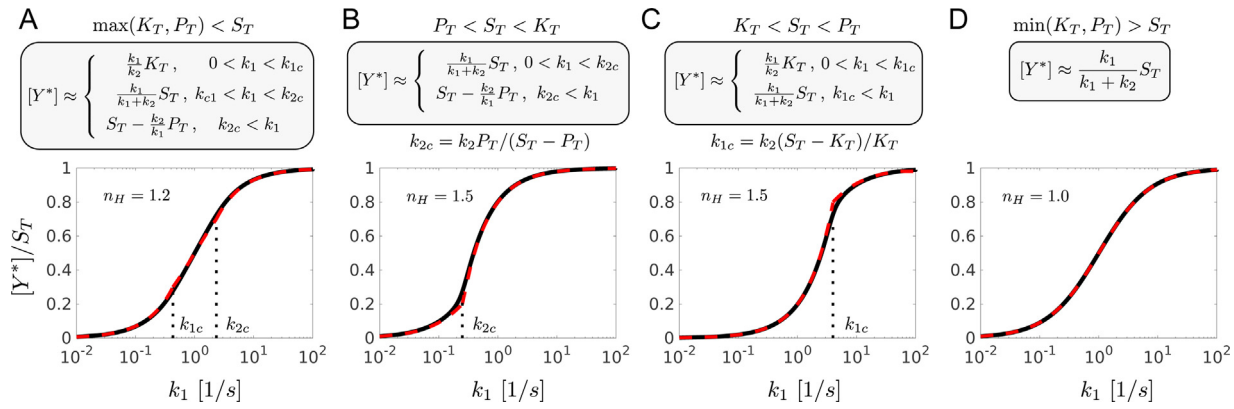

Fig. 9. Steady state operating regimes of covalent modification cycles under the conditions of enzyme excess ($K_T + P_T > S_T$) and enzyme saturation ($K_1 \ll K_T$ and $K_2 \ll P_T$). The Hill coefficient $n_H = \ln 81/\ln R_S$ is defined in terms of the response coefficient $R_S = k_1^{(90)}/k_1^{(10)}$ which is given by the ratio of parameter values that elicit 90% (and 10%) of the maximal response. Red dashed lines correspond to the approximate solutions shown above each panel. Parameters: (A) $K_T = P_T = 0.7$ μM, (B) $K_T = 2$ μM, $P_T = 0.2$ μM, (C) $K_T = 0.2$ μM, $P_T = 2$ μM, (D) $K_T = P_T = 2$ μM. Other parameters: $S_T = 1$ μM, $K_1 = K_2 = 0.01$ μM, $k_2 = 1$/s. (For interpretation of the references to color in this figure legend, the reader is referred to the web version of this article.)

where covalent modification cycles exhibits both enhanced sensitivity and concentration robustness (Fig. 9B and C).

To describe the effect of genetic perturbations one is often interested in $[Y^*]$ as a function of the total substrate concentration S_T. One can show that in this case the shape of the response curve depends on the ratio α of the maximal reaction rates of kinase and phosphatase (Eq. (45)). If $\alpha > 1$ ($\alpha < 1$) the response curve is monotonically increasing (decreasing) and if both converter enzymes operate in opposite regimes it may also change in a non-monotonic manner (Straube, 2017).

3.3. Substrate competition

Apart from the zero-order effect substrate competition represents an alternative mechanism for the generation of ultrasensitivity in regulatory networks. First experimental evidence for this effect came from studies of Kim and Ferrell who showed that the phosphorylation level of the mitotic regulator Wee1 exhibits a sharp threshold and ultrasensitivity to changes in the concentration of Cdk1 (Kim and Ferrell, 2007). The latter is a cell-cycle related kinase that is estimated to have about 200 substrates in budding yeast (Ubersax et al., 2003; Enserink and Kolodner, 2010). Interestingly, the ultrasensitive response could be reproduced in a reconstituted system by adding a different high-affinity Cdk1 substrate. However, in the absence of such substrates the response of phosphorylated Wee1 was hyperbolic suggesting that the observed ultrasensitivity did not arise from the zero-order effect rather than from the competition between Wee1 and alternative Cdk1 substrates.

To describe competition effects in phosphorylation/dephosphorylation cycles Ferrell and Ha proposed a model (Ferrell and Ha, 2014) where two substrates (X and Y) are phosphorylated by a single kinase (K) according to a Michaelis–Menten scheme whereas dephosphorylation was assumed to occur by an auxiliary phosphatase in a first-order process (Fig. 10A). Interestingly, the analysis of this system yields a cubic steady state equation for the phosphorylation level of the low-affinity substrate that is structurally similar to Eq. (35) (Straube, 2015). Hence, one can expect the same type of input–output behaviors as in the case of receptor–ligand binding, i.e. hyperbolic, threshold-hyperbolic and ultrasensitive responses. To analyze a particular limiting regime one may use the approximations derived in Eqs. (37) and (38), and substitute the parameters in these equations by those corresponding to covalent modification cycles (cf. Table 1).

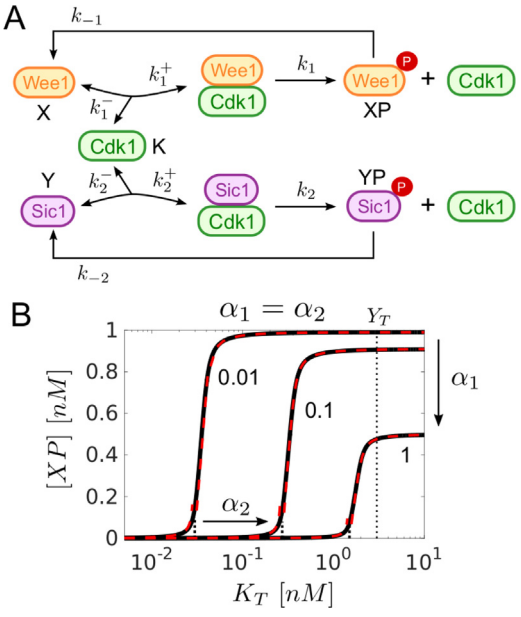

Fig. 10. Substrate competition in phosphorylation/dephosphorylation cycles. (A) Two substrates (X and Y) compete for access to Cdk1 (K) which mediates phosphorylation of Wee1 and Sic1. Dephosphorylation is assumed to follow pseudo first-order kinetics. (B) Steady state concentration of the phosphorylated form of the low-affinity substrate as a function of the kinase concentration in the ultrasensitive regime. As $\alpha_1 = k_{-1}/k_1$ and $\alpha_2 = k_{-2}/k_2$ are simultaneously increased from 0.01 to 1 the threshold $K_T^* = \alpha_2 Y_T/(1+\alpha_2)$ (short dotted lines) increases and the maximal amplitude $[XP]_{\max} = X_T/(1+\alpha_1)$ decreases while the steepness of the response curve remains the same. Red dashed lines were computed from Eq. (57). Parameters: $K_1 = 0.1$ nM, $K_2 = 10^{-3}$ nM, $X_T = 1$ nM, $Y_T = 1$ nM, $k_1 = k_2 = 1$/s. (For interpretation of the references to color in this figure legend, the reader is referred to the web version of this article.)

Table 1
Parameter substitutions for systems with substrate competition as described by Eq. (35).

Receptor–ligand binding	Covalent modification cycles	Two-component systems
$[L1.R]$	$[XP]$	$[RR1^*]$
R_T	$\frac{K_T}{\alpha_1}$	$C_{p,1}$
$L2_T$	$\frac{\alpha_2}{\alpha_1}\frac{Y_T}{1+\alpha_2}$	$\frac{C_{p,1}}{C_{p,2}} RR_{2T}$
$L1_T$	$\frac{X_T}{1+\alpha_1}$	RR_{1T}
K_{d1}	$\frac{K_1}{1+\alpha_1}$	$C_{t,1}$
$\frac{K_{d2}}{K_{d1}}$	$\frac{K_2}{K_1}\frac{\alpha_2}{1+\alpha_2}\frac{1+\alpha_1}{\alpha_1}$	$\frac{C_{p,1}}{C_{p,2}}/\frac{C_{t,1}}{C_{t,2}}$

For example, in phosphorylation/dephosphorylation cycles the limit of strong substrate competition is defined by

$$\varepsilon \cdot \beta \ll 1 \tag{56}$$

where $\varepsilon = K_2/K_1$ represents the ratio between the Michaelis–Menten constants of the two substrates and

$$\beta = \frac{\alpha_2}{1+\alpha_2}\frac{1+\alpha_1}{\alpha_1}, \alpha_i = \frac{k_{-i}}{k_i}, i = 1, 2$$

represents a scale factor that involves ratios between the catalytic rates of phosphorylation and dephosphorylation of the two substrates (cf. Fig. 10A). Under the condition in Eq. (56) the phosphorylation level of the low-affinity substrate can be approximated by

$$[XP] \approx \begin{cases} \varepsilon\beta\dfrac{X_T}{1+\alpha_1}\dfrac{K_T}{K_T^* - K_T}, & K_T < K_T^* \\ [XP]_-, & K_T > K_T^* \end{cases} \tag{57}$$

where

$$K_T^* = \frac{\alpha_2}{1+\alpha_2}Y_T$$

defines a threshold concentration and $[XP]_-$ is given by the negative root of the **LR**-type equation (cf. Eq. (38))

$$x^2 - \left(\frac{K_T - K_T^*}{\alpha_1} + \frac{X_T + K_1}{1+\alpha_1}\right)x + \frac{K_T - K_T^*}{\alpha_1}\frac{X_T}{1+\alpha_1} = 0.$$

Using the parameter substitutions in Table 1 one can predict that the response curve increases hyperbolically beyond the threshold if $K_1 \gg X_T$ whereas an ultrasensitive response requires $K_2 \ll K_1 \ll X_T$. Compared to the case of receptor–ligand binding both the threshold and the maximal phosphorylation level of the low-affinity substrate depend on the kinetic parameters of phosphorylation and dephosphorylation. Specifically, increasing α_2 increases the threshold while increasing α_1 lowers the maximal phosphorylation level (Fig. 10B).

3.4. Bifunctional converter enzymes

In some cases the activities of the two opposing enzymes in a covalent modification cycle are located on the same protein in which case modification and demodification are carried out by a single *bifunctional* enzyme. Prominent examples are the isocitrate dehydrogenase kinase/phosphatase (IDHKP) involved in the regulation of the tricarboxylic acid cycle (LaPorte and Koshland, 1982), the uridylyltransferase involved in nitrogen assimilation in *E. coli* (Garcia and Rhee, 1983; Ninfa et al., 2000) and the mammalian 6-phosphofructo-2-kinase/fructose-2,6-bisphosphatase which integrates multiple signals to regulate the switch between glycolysis and gluconeogenesis in the liver (Kurland and Pilkis, 1995; Dasgupta et al., 2014).

Originally, it was believed that bifunctional enzymes mediate graded responses and robustness rather than ultrasensitivity (Ortega et al., 2002; Shinar et al., 2007, 2009; Hart et al., 2011a,b; Dexter and Gunawardena, 2013). The latter property can be readily understood from the observation that the enzyme concentration cancels out from the steady state equation (Eq. (44)) because it appears in the forward (K_T) as well as in the backward rate (P_T). Hence, for bifunctional enzymes (with $K_T = P_T$) the parameter $\alpha = k_1K_T/(k_2P_T) = k_1/k_2$ becomes independent of the enzyme concentration so that changes in the latter would not affect the stimulus-response curves in Fig. 8. This form of concentration robustness has been related to structural properties of a network (Shinar and Feinberg, 2010) or to the existence of certain algebraic invariants (Dexter et al., 2015). More generally, robustness properties can be understood in terms of parameter non-identifiability (Sontag, 2017).

Concentration robustness may not only occur with respect to the enzyme concentration, but also to that of substrates and/or effectors. Interestingly, this can happen already at the level of the Goldbeter–Koshland model in the signal-transducing regime. To see this more explicitly, we rewrite the approximation for the stimulus-response curve (Fig. 8D) as a function of the substrate concentration, i.e.

$$[S^*] \approx \begin{cases} S_T\left(1 - \dfrac{K_1}{\alpha K_2 - S_T}\right), & S_T < \alpha K_2 \\ \alpha K_2, & S_T > \alpha K_2 \end{cases} \tag{58}$$

Hence, if $S_T > \alpha K_2$ the concentration of the phosphorylated substrate becomes independent of the substrate concentration ($[S^*] \approx \alpha K_2$) so that $[S^*]$ exhibits concentration robustness with respect to S_T in that regime.

Yet, there were known examples of demonstrated ultrasensitivity for bifunctional enzymes (Fig. 11A) raising the question how one can understand the emergence of ultrasensitivity in bifunctional enzyme systems (Straube, 2012). In fact, the first experimental evidence for enhanced sensitivity in covalent modification cycles came from studies with the bifunctional IDHKP (LaPorte and Koshland, 1983) although the measured stimulus-response curve (Fig. 11B) more resembled that of a linear-saturation response as it occurs in the signal-transducing regime (Fig. 8D). Interestingly, both behaviors can be understood within a common mechanistic model which was originally proposed by Shinar et al. (2009) to describe IDHKP-mediated robustness in glyoxylate bypass regulation (LaPorte et al., 1985). Later, it was shown by means of a rapid equilibrium approximation that the Shinar model yields a **GK**-type equation (Straube, 2013) if one replaces in Eq. (44) Michaelis–Menten constants by dissociation constants. Hence, if a bifunctional enzyme exhibits two distinct catalytic sites for its opposing activities one may expect similar types of stimulus-response curves as for covalent modification cycles with distinct converter enzymes (Fig. 8) including ultrasensitivity and concentration robustness where the latter occurs in the signal-transducing regime (Eq. (58)). In support of this expectation evidence for concentration robustness has recently been observed in the regulation of cellular Pi homeostasis by PPIP5K which denotes a family of bifunctional enzymes with two domains for its kinase and phosphatase activities (Gu et al., 2017).

3.4.1. Bifunctional enzymes with a single catalytic site

Although many bifunctional enzymes seem to exhibit distinct catalytic sites for their opposing activities there are examples where modification and demodification are carried out by a single catalytic center. The most prominent members of this class are sensor histidine kinases which are part of two-component systems (cf. Section 4). Based on the crystal structure it seems that also the IDHKP exhibits just a single catalytic site (Zheng and Jia, 2010) which would prevent formation of a ternary $S - KP - S^*$ complex as assumed in the Shinar model (Fig. 11C). This leads to the strange situation that, though the predictions based on this model quantitatively agree with the measured stimulus-response curve (Fig. 11B) it mechanistically does not apply to the case of the IDHKP. However, a revised model taking into account the structure of the active site as well as substrate dimerization confirms the existence of concentration robustness for the IDH cycle (Dexter and Gunawardena, 2013).

Apart from concentration robustness one might ask whether bifunctional enzymes with a single catalytic site may also yield ultrasensitivity? It turns out that this is, indeed, the case if one assumes that the opposing activities are reciprocally regulated by

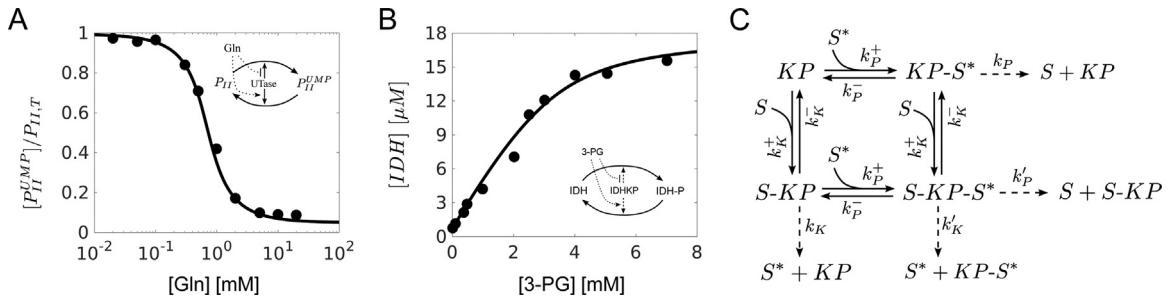

Fig. 11. Ultrasensitivity in covalent modification cycles with a bifunctional converter enzyme. (A) Ultrasensitive response in the uridylylation of the PII protein (also known as GlnK) by the uridylyltransferase (UTase) which is reciprocally regulated by glutamine (Gln). (B) Isocitrate dehydrogenase (IDH) exhibits a linear-saturation response as a function of 3-PG which reciprocally regulates the isocitrate dehydrogenase kinase/phosphatase (IDHKP). Circles represent experimental results from Ventura et al. (2010) (A) and LaPorte and Koshland (1983) (B). Solid lines were computed based on the reaction network depicted in panel C using experimentally measured values (Straube, 2013). (C) Reaction mechanism for the phosphorylation of a substrate S by a bifunctional enzyme with two catalytic sites according to Shinar et al. (2009).

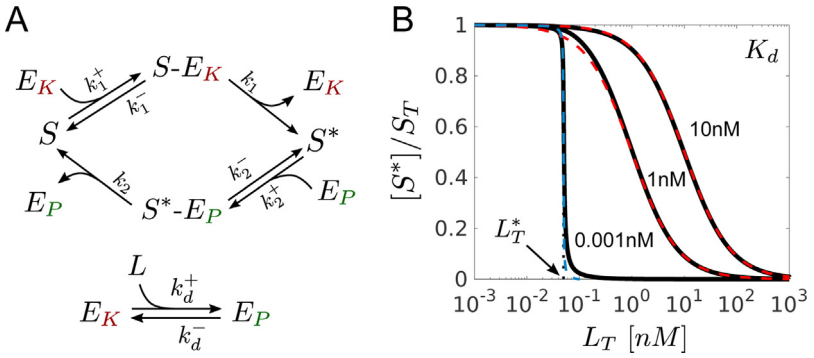

Fig. 12. Reciprocal regulation in covalent modification cycles with a bifunctional converter enzyme. (A) Reaction mechanism for an enzyme with a single catalytic site. E_K and E_P denote enzyme states in kinase and phosphatase mode, respectively. Binding of a ligand L to E_K is assumed to switch the enzyme into phosphatase mode. (B) Stimulus-response curves for increasing binding affinity. At low affinity $K_d \gg E_T$ ($K_d = k_d^-/k_d^+$) the response is graded, at high affinity ($K_d \ll E_T$) the response becomes highly ultrasensitive, but is restricted to $L_T < E_T$. Dashed curves were computed from Eqs. (59) (red) and (60) (blue). Parameters: $E_T = 0.1$ nM, $S_T = 10$ nM, $K_1 = K_2 = 0.1$ nM, $k_1 = k_2 = 1$/s. (For interpretation of the references to color in this figure legend, the reader is referred to the web version of this article.)

an allosteric effector (Fig. 12A). To this end, we assume that the enzyme may exist in a kinase state (E_K) and in a phosphatase state (E_P), and that binding of the effector to the kinase state switches it from kinase to phosphatase mode. Interestingly, the response behavior of such a system depends on the affinity of the effector (Straube, 2014). If the affinity is low ($K_d \gg E_T$) the concentration of the phosphorylated form of the substrate exhibits a hyperbolic dependence on the effector concentration as described by

$$[S^*] \approx \frac{S_T}{1 + \frac{k_2/K_2 L_T}{k_1/K_1 K_d}}. \tag{59}$$

Here, K_1 and K_2 denote respectively the Michaelis–Menten constants associated with the kinase and the phosphatase activity, and $K_d = k_d^-/k_d^+$ denotes the dissociation constant of the enzyme-effector complex. In contrast, if the enzyme exhibits a high affinity for the effector ($K_d \ll E_T$) the steady state is determined a **GK**-type equation of the form

$$k_1 (E_T - L_T) \frac{S_T - [S^*]}{K_1 + S_T - [S^*]} \approx k_2 L_T \frac{[S^*]}{K_2 + [S^*]} \tag{60}$$

where $E_T - L_T$ and L_T play the role of an effective kinase and phosphatase concentration, respectively. In this regime bifunctional enzymes with a single catalytic site may generate similar response behaviors as covalent modification cycles with distinct converter enzymes. However, this regime is restricted to low effector concentration ($L_T < E_T$) where the enzyme is not saturated by the effector.

4. Two-component signal transduction

Two-component systems (TCSs) are modular signal transduction systems which are utilized by bacteria and other microbes to sense and respond to diverse stimuli (Stock et al., 2000) such as osmolarity (EnvZ/OmpR), magnesium limitation (PhoQ/PhoP) or nitrogen assimilation (NtrB/NtrC). While *E. coli* comprises about 30 TCSs, other bacteria express more than 100 of these systems (Alm et al., 2006). Canonical TCSs consist of a sensor histidine kinase (HK) and a cognate response regulator (RR) which often acts as a transcription factor to activate or repress a particular set of response genes. The HK exhibits up to three distinct activities to modulate the RR phosphorylation level: Upon stimulation, the HK autophosphorylates at a conserved histidine residue and transfers the phosphoryl group to an aspartate residue in the RR receiver domain. The unphosphorylated form of the HK often exhibits a distinct phosphatase activity towards the phosphorylated form of RR endowing many HKs with a bifunctional design (Goulian, 2010).

4.1. The Batchelor–Goulian model

More than 20 years ago Russo and Silhavy argued that if HK autophosphorylation represents the rate-limiting step in RR phosphorylation TCSs with a bifunctional design should exhibit special robustness properties. Specifically, the RR phosphorylation level should be approximately independent with respect to variations in both the concentration of the HK and that of the RR (Russo and Silhavy, 1993). Ten years later, by measuring the transcriptional activity of OmpR-regulated genes, Batchelor and Goulian provided the first experimental evidence for concentration robust-

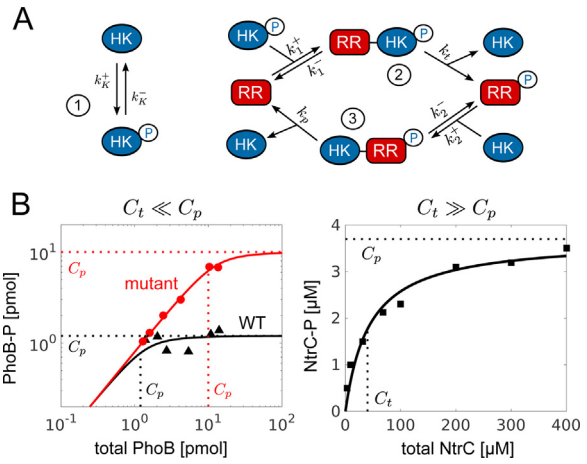

Fig. 13. Concentration robustness in the Batchelor–Goulian model. (A) Reaction scheme includes HK autophosphorylation (1), phosphotransfer (2) and HK phosphatase activity (3). (B) Comparison of the Batchelor–Goulian model with measurements of the RR phosphorylation level as a function of total RR abundance. Left panel: PhoR/PhoB system (Gao and Stock, 2013). The mutant PhoB exhibits reduced affinity for PhoR which increases the value of C_p. The stimulus-response curves are of linear-saturation type as predicted by Eq. (63). Right panel: NtrB/NtrC system (Jiang et al., 2012). The stimulus-response curve exhibits a Michaelian shape as predicted by Eq. (64).

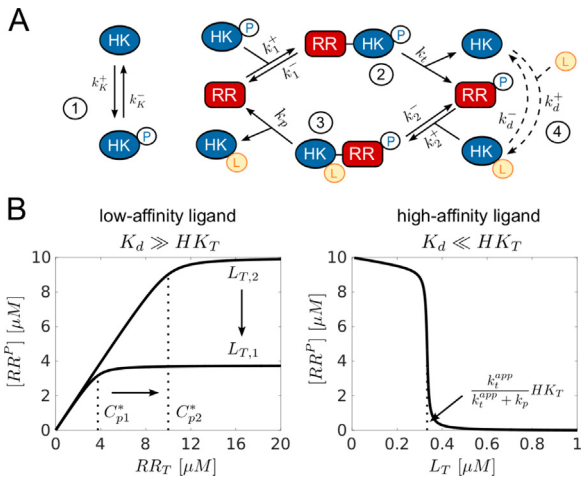

Fig. 14. Reciprocal regulation in two-component systems. (A) Binding of a ligand (4) inhibits autophosphorylation (1) and phosphotransfer (2), but activates the HK's phosphatase activity (3). (B) Depending on the binding affinity of the ligand ($K_d = k_d^-/k_d^+$) the system may either exhibit concentration robustness (left panel) or zero-order ultrasensitivity (right panel).

ness in TCSs (Batchelor and Goulian, 2003). They also proposed a simple model that could qualitatively account for the observed robustness under variations of RR and HK abundances (Fig. 13A). Under conditions when the HK is much less abundant than the RR (which is the typical situation in TCSs) the steady states within the Batchelor–Goulian model are determined by the **LR**-type equation (cf. Eq. (8))

$$[RR^*]^2 - \left(C_p + RR_T + C_t\right)[RR^*] + C_p RR_T \approx 0 \tag{61}$$

where RR^* stands for the phosphorylated form of the RR,

$$C_p = \frac{k_K^+}{k_p} K_p \text{and} C_t = \frac{k_K^-}{k_t} K_t \tag{62}$$

denote rescaled Michaelis–Menten constants associated with the phosphatase and the kinase activities of the HK, and RR_T denotes the total RR concentration. In the 'high-affinity' limit, defined by $C_t \ll C_p$, the solution of Eq. (61) can be approximated by

$$[RR^*] \approx \begin{cases} RR_T, & RR_T < C_p \\ C_p, & RR_T > C_p \end{cases} \tag{63}$$

i.e. if the concentration of the RR exceeds the threshold C_p its level remains approximately constant. Note that the value of this constant (C_p) only depends on kinetic parameters, but not on protein concentrations (Eq. (62)). In the 'low-affinity' regime, defined by $C_t \gg C_p$, the solution of Eq. (61) can be approximated by

$$[RR^*] \approx \frac{C_p RR_T}{C_p + RR_T + C_t}. \tag{64}$$

Interestingly, both types of behaviors were observed experimentally (Fig. 13B). The Batchelor–Goulian model has also been used to model other regulatory aspects of TCSs such as the impact of autoregulation (Miyashiro and Goulian, 2008) and the emergence of cross-talk (Siryaporn et al., 2010). However, there also exist alternative TCS models which describe, for example, phosphotransfer as a reversible reaction (Kremling et al., 2004; Tindall et al., 2013) or include the formation of dead-end complexes (Igoshin et al., 2008).

4.2. Reciprocal regulation of HK activities

A quantitative analysis of the input–output behavior of TCSs is often limited by the fact that the physiological signal sensed by the HK is not well known (Krell et al., 2010). In cases where the signal has been identified it became evident that the HK's autokinase and phosphatase activities are the primary targets of regulation (Stewart, 2010; Heermann and Jung, 2010) and that regulation of these activities often occurs in a reciprocal manner (Jiang and Ninfa, 1999; Chamnongpol et al., 2003; Dubey et al., 2016). Figure 14A shows an example where binding of an allosteric ligand switches the HK from kinase to phosphatase mode, i.e. in the presence of the signal the system is shut-off and only when the signal becomes limiting the system is switched on. Similar regulatory structures have been observed in the PhoQ/PhoP and NtrB/NtrC systems (Jiang and Ninfa, 1999; Chamnongpol et al., 2003).

Similar as in the case of covalent modification cycles with a bifunctional converter enzyme (cf. Fig. 12) the steady state behavior of a TCS with reciprocal regulation depends on the affinity of the ligand. If the affinity is low ($K_d \gg HK_T$) the steady state equation becomes identical with the **LR**-type equation in Eq. (61) if C_p is replaced by $C_p^* = C_p K_d / L_T$ where L_T denotes the total ligand concentration and $K_d = k_d^-/k_d^+$ denotes the dissociation constant for ligand binding. Hence, in this regime the threshold for reaching a constant phosphorylation level as well as the value of this constant depend on the ligand concentration (Fig. 14B, left panel), i.e. the system exhibits stimulus-dependent concentration robustness (Straube, 2014). In contrast, if the ligand exhibits a high affinity for the HK the steady state is determined by a **GK**-type equation

$$k_t^{app}(HK_T - L_T)\frac{RR_T - [RR^*]}{K_t^{app} + RR_T - [RR^*]} \approx k_p L_T \frac{[RR^*]}{K_p + [RR^*]} \tag{65}$$

where K_P denotes the Michaelis–Menten constant associated with the phosphatase activity of the HK and

$$k_t^{app} = \frac{k_t}{1 + k_t/k_K^+} \text{and} K_t^{app} = K_t \frac{1 + k_K^-/k_K^+}{1 + k_t/k_K^+}$$

denote apparent constants that can be expressed in terms of rate constants and the Michaelis–Menten constant associated with the phosphotransferase activity (K_t). Hence, when triggered by a high-affinity ligand TCSs may behave similarly to covalent modification cycles and exhibit zero-order ultrasensitivity to input signals

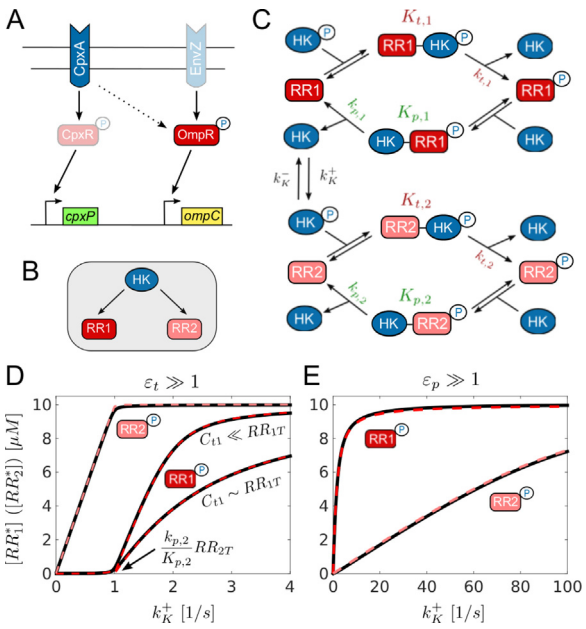

Fig. 15. Cross-talk and substrate competition in two-component systems. (A) *In vivo*, cross-talk from CpxA to OmpR is only observable in the absence of CpxR and EnvZ (Siryaporn and Goulian, 2008). (B) Cross-talk motif: 1HK phosphorylates to RRs. (C) Detailed model for the motif in B. (D) If the HK exhibits a kinetic preference for RR2 with respect to its phosphotransferase activity ($\varepsilon_t \gg 1$) RR2 becomes insulated and $\left[RR_1^*\right]$ exhibits a threshold in the response curve. Parameters: $K_{p,1} = K_{p,2} = 1\ \mu M$, $k_{p,1} = k_{p,2} = k_{t,1} = 0.1/s$, $k_{t,2} = 1/s$. Lower curve: $K_{t,1} = 10\ \mu M$, $K_{t,2} = 0.1\ \mu M$. Upper curves: $K_{t,1} = 1\ \mu M$, $K_{t,2} = 0.01\ \mu M$. Dashed curves were computed from Eqs. (66), (67) and (68). (E) If the HK exhibits a kinetic preference for RR2 with respect to its phosphatase activity ($\varepsilon_p \gg 1$) RR2 becomes insulated, but the non-cognate RR (RR1) becomes phosphorylated first. Parameters: $K_{t,1} = K_{t,2} = 1\ \mu M$, $k_{t,1} = k_{t,2} = k_{p,1} = 0.1/s$, $k_{p,2} = 1/s$, $K_{p,1} = 1\ \mu M$, $K_{p,2} = 0.1\ \mu M$. Dashed curves were computed from Eqs. (69) and (66). Other parameters: $RR_{1T} = RR_{2T} = 10\ \mu M$, $k_K^- = 0.1/s$.

(Fig. 14B, right panel). In this regime TCSs may even exhibit bistability if ultrasensitivity is combined with a positive feedback loop, e.g. due to autoregulation of the HK and RR genes (Wei et al., 2014). However, as can be seen from Eq. (65) the occurrence of ultrasensitivity is restricted to ligand concentrations that are lower than that of the sensor kinase (such that $HK_T - L_T > 0$) making this operating regime particularly useful to detect and amplify low-abundant input signals.

4.3. Cross-talk

New input–output functionality of TCSs is often acquired through gene duplication and subsequent divergence of paralogous genes (Alm et al., 2006; Capra et al., 2012). As a result, many sensor kinases do not only phosphotransfer to their cognate response regulator, but (on longer time scales) also to those of other TCSs (Fisher et al., 1996; Skerker et al., 2005). However, *in vivo* cross-talk from a HK to a non-cognate RR seems to be extremely rare being only observable after the cognate RR and the non-cognate HK have been genetically eliminated (Fig. 15A) (Siryaporn and Goulian, 2008; Groban et al., 2009). To ensure this high degree of specificity three main mechanisms have been identified: molecular recognition, phosphatase activity of the HK and substrate competition (Podgornaia and Laub, 2013). Among these mechanisms molecular recognition appears to be the most dominant one. Experiments have shown that the specificity constant of a HK as measured by the k_{cat}/K_M ratio is $10^4 - 10^5$ times higher for the cognate RR (Fisher et al., 1996; Grimshaw et al., 1998; Skerker et al., 2005) implying a huge kinetic preference of a HK for its cognate RR. In fact, mathematical modeling has suggested that there is a strong selective pressure to eliminate cross-talk between TCSs after gene duplication before new input–output functionality can be acquired (Rowland and Deeds, 2014).

To understand how a strong kinetic preference may generate pathway insulation within the Batchelor–Goulian model we consider the case where one HK phosphorylates its cognate partner (RR2) and a non-cognate regulator denoted by RR1 (Fig. 15B and C). The steady state equation for the phosphorylated form of RR1 is a cubic polynomial that is structurally similar to Eq. (35) (cf. Supporting Information and Table 1). Its steady state behavior depends on whether the HK exhibits a kinetic preference (for RR2) with respect to its phosphotransferase activity ($\varepsilon_t \gg 1$) or with respect to its phosphatase activity ($\varepsilon_p \gg 1$) where ε_t and ε_p are defined by (cf. Fig. 15C)

$$\varepsilon_t = \frac{k_{t,2}/K_{t,2}}{k_{t,1}/K_{t,1}} \text{and} \varepsilon_p = \frac{k_{p,2}/K_{p,2}}{k_{p,1}/K_{p,1}}.$$

In the first case ($\varepsilon_t \gg 1$) the steady states for $\left[RR_2^*\right]$ and $\left[RR_1^*\right]$ are determined (to leading order) by the **LR**-type equations

$$\left[RR_2^*\right]^2 - \left[RR_2^*\right]\left(RR_{2T} + C_{p,2} + C_{t,2}\right) + C_{p,2}RR_{2T} \approx 0 \tag{66}$$

and

$$\left[RR_1^*\right]^2 - \left(RR_{1T} + C_{p,1}^{\text{eff}} + C_{t,1}\right)\left[RR_1^*\right] + C_{p,1}^{\text{eff}}RR_{1T} \approx 0 \tag{67}$$

where $C_{p,1}^{\text{eff}} = C_{p,1} - \varepsilon_p RR_{2T}$. Hence, the cognate RR (RR2) behaves as if the non-cognate partner was absent while the latter may exhibit threshold behavior if $C_{t,1} \ll RR_{1T}$. For autophosphorylation rates below a threshold the phosphorylation level of RR_1^* remains low, too, i.e.

$$\left[RR_1^*\right] \approx \frac{1}{\varepsilon_t}\frac{RR_{1T}C_{p,1}}{RR_{2T} - C_{p,2}}, k_K^+ < \frac{k_{p,2}}{K_{p,2}}RR_{2T}, \tag{68}$$

beyond the threshold it increases either hyperbolically ($C_{t1} \gg RR_{1T}$) or in an ultrasensitive manner ($C_{t1} \ll RR_{1T}$) (Fig. 15D).

In contrast, if the HK develops a kinetic preference with respect to its phosphatase activity ($\varepsilon_p \gg 1$) the steady state for $\left[RR_2^*\right]$ is still determined by Eq. (66) while that for $\left[RR_1^*\right]$ is determined by a different **LR**-type equation

$$\left[RR_1^*\right]^2 - \left(RR_{1T} + C_{p,1} + C_{t,1}^{\text{eff}}\right)\left[RR_1^*\right] + C_{p,1}RR_{1T} \approx 0 \tag{69}$$

where $C_{t,1}^{\text{eff}} = C_{t,1} + \varepsilon_t RR_{2T}$. In that case no threshold exists and the order in which the RRs are phosphorylated is reversed. As a result the non-cognate RR becomes fully phosphorylated already at low autophosphorylation rates (Fig. 15E). Together this suggests that to insulate newly emerging TCSs developing a kinetic preference with respect to the phosphotransferase rather than the phosphatase activity should be the better strategy which is supported by the fact that the latter has not been observed experimentally yet (Siryaporn and Goulian, 2008).

In some cases cross-talk where two RRs are phosphorylated by a single HK may be a desirable feature of a regulatory network in which case it has been referred to as cross-regulation (Laub and Goulian, 2007). For example, in the chemotaxis network of *E. coli* the histidine kinase CheA can phosphorylate either of the two regulator proteins CheY and CheB: while CheY-P controls the sense of rotation of the flagellar motor CheB-P mediates feedback regulation at the receptor level (Sourjik, 2004). Also, since the threshold for the non-cognate partner depends on the concentration of the cognate RR (Eq. (68)) the 1HK/2RR motif (Fig. 15B) has been suggested as a basis for constructing a tunable threshold device in the context of synthetic biology applications (Amin et al., 2014).

5. Conclusions

In physics, the superior importance of the harmonic oscillator derives from its repeated occurrence in different branches of physics which allows describing diverse phenomena such as vibrational modes in solid states or oscillations in electrical circuits using similar equations. In this review we advocated the opinion that, as far as the steady state behavior is concerned, elementary network motifs might play a similar role for understanding the behavior of larger biological networks. We have illustrated this approach starting from a simple bimolecular reaction and adding successively more complexity such as substrate competition, cooperativity or covalent modifications. If analyzed in the limit of strong or weak coupling (e.g. high or low affinity of a ligand) or under conditions of substrate excess the corresponding steady state equations became structurally similar to those of a bimolecular reaction (**L**-type and **LR**-type equations) or to that of the Goldbeter–Koshland model describing covalent modifications (**GK**-type equation).

Different limits may lead to different equations as in the case of two-component systems where the sensor kinase is reciprocally regulated by an allosteric effector (Fig. 14): If the affinity of the effector is high the system is described by an equation of the Goldbeter–Koshland type (Eq. (65)); in the low-affinity limit it becomes similar to that of a bimolecular reaction (Eq. (61)). In these equations the parameters of the elementary motifs are typically replaced by parameters with a different meaning or by parameter combinations. In the latter case information from different parts of the network is condensed into few effective parameters (cf. Table 1) which allows for a quantitative understanding of signal integration.

Despite the fact that different systems can be described by similar equations the interpretation of the resulting input–output behavior might be different. For example, under conditions of substrate excess two-component systems can be described by a similar equation as receptor–ligand binding. However, for two-component systems the receptor concentration is replaced by a rescaled Michaelis–Menten constant which only depends on kinetic parameters of the system. As a consequence the stimulus-response curve for receptor–ligand binding describes saturation of a receptor by a ligand while that for a two-component system describes concentration robustness (Fig. 13).

5.1. Challenges and future directions

In this review we focused on the simplest network motifs within each class, e.g. two ligands competing for a binding site on a receptor, for which analytical results are known. However, *in vivo* the number of competitors could be substantially higher which may lead to multiple thresholds and hierarchical regulation (Levine et al., 2007; Mitarai et al., 2007). As the number of competitors increases the polynomial order of the corresponding steady state equations increases, too. To systematically derive and analyze such equations algebraic approaches have proven to be useful (Thomson and Gunawardena, 2009; Feliu et al., 2012; Estrada et al., 2016). When going from 2 to n competitors or from one covalent modification cycle to n such cycles, as in a MAP kinase cascade, it will be interesting to see if the resulting steady state equations can still be reduced to a **L**-type, **LR**-type or **GK**-type equation. If so, this may provide a classification of network architectures based on their decomposability into elementary network motifs. One could also envision a classification where larger networks, that can be described by the same equation as an elementary network motif, may be replaced by an 'equivalent circuit' of the motif with renormalized input–output parameters similar as for electrical circuits. Such a classification would be particularly useful to aid the construction and integration of novel regulatory circuits in the context of synthetic biology.

While this review almost exclusively focused on steady state aspects of regulatory networks it remains a major challenge to decode the information processed by cells that is encoded in the temporal response of a network (Sasagawa et al., 2005; Thurley et al., 2012; Levine et al., 2013). For example, the physiological response may depend on whether a steady state is approached monotonically or through relaxation after an overshoot (Shin et al., 2006). In ODE systems with two or more state variables a steady state may become unstable in a Hopf bifurcation giving rise to sustained oscillations which encode information in their shape and their frequency. Similar as for steady states an approach based on network motifs was used to classify biological oscillators (Novak and Tyson, 2008). At least close to bifurcation points the transient dynamics of such systems can be described by 'normal form' equations which contain only a few effective parameters (Kuznetsov, 1998). Away from bifurcation points systems typically have to be analyzed on a case by case basis, and it remains an open question whether the transient dynamics of larger networks can be understood in terms of the known behavior of some elementary motifs. However, model reduction techniques such as the total QSSA may provide a suitable starting point for a systematic analysis.

Appendix A. Approximations for τ_s

A.1 Approximations for τ_s

If $K_d \ll |L_T - R_T|$ and $L_T \neq R_T$ we can approximate τ_s, defined in Eq. (9), by

$$\begin{aligned}\tau_s &= \frac{K_d}{k_d^- \sqrt{(L_T-R_T)^2 + 2K_d(L_T+R_T) + K_d^2}} \\ &\approx \frac{K_d}{k_d^- |L_T-R_T| \sqrt{1 + 2\frac{K_d(L_T+R_T)}{(L_T-R_T)^2}}} \\ &\approx \frac{1}{k_d^+ |L_T-R_T|}\left(1 - \frac{K_d(L_T+R_T)}{(L_T-R_T)^2}\right)\end{aligned} \tag{70}$$

where we have used that $\sqrt{1+x} \approx 1 + x/2$ and $1/(1+x) \approx 1 - x$ when $x \ll 1$. For $L_T = R_T$ the leading order diverges and we obtain from Eq. (70)

$$\begin{aligned}\tau_s &= \frac{K_d}{k_d^- \sqrt{4K_dR_T + K_d^2}} = \frac{1}{k_d^-} \frac{\sqrt{\frac{K_d}{4R_T}}}{\sqrt{1 + \frac{K_d}{4R_T}}} \\ &\approx \frac{1}{k_d^-}\sqrt{\frac{K_d}{4R_T}}\left(1 - \frac{K_d}{8R_T}\right).\end{aligned}$$

In the limit $K_d \gg \max(L_T, R_T)$ we approximate τ_s by

$$\begin{aligned}\tau_s &= \frac{1}{k_d^- \sqrt{1 + 2\frac{L_T+R_T}{K_d} + \left(\frac{L_T-R_T}{K_d}\right)^2}} \\ &\approx \frac{1}{k_d^-\left(1 + \frac{L_T+R_T}{K_d}\right)}\end{aligned}$$

which agrees with the expression in Eq. (13).

A.2 Approximations for the cooperative binding motif

A.2.1 Positive cooperativity

In the limit of strong positive cooperativity ($c \gg b$) we rewrite Eq. (27) in the form

$$x^2 - (K_{1T} + K_{2T} + \varepsilon S_T)x + (1+\varepsilon)K_{1T}K_{2T} = 0 \tag{71}$$

where

$$\varepsilon = \frac{b}{c-b} \ll 1.$$

For fixed $S_T \sim \mathcal{O}(K_{1T}, K_{2T})$ substituting the Ansatz

$$x = x_0 + \varepsilon x_1 + \mathcal{O}\left(\varepsilon^2\right)$$

into Eq. (71) yields

$$x_0^2 - (K_{1T} + K_{2T})x_0 + K_{1T}K_{2T} = 0 \tag{72}$$

and

$$2x_0x_1 - (K_{1T} + K_{2T})x_1 - S_Tx_0 + K_{1T}K_{2T} = 0. \tag{73}$$

Since $x \leq \min(K_{1T}, K_{2T})$ the solution of Eq. (72) is given by

$$x_0 = \frac{K_{1T} + K_{2T}}{2} - \frac{\left|K_{1T} - K_{2T}\right|}{2} = \begin{cases} K_{1T} & K_{1T} < K_{2T} \\ K_{2T} & K_{1T} > K_{2T} \end{cases}$$

Substituting this solution into Eq. (73) and solving for x_1 gives

$$x_1 = \begin{cases} -K_{1T}\dfrac{S_T - K_{2T}}{K_{2T} - K_{1T}}, & K_{1T} < K_{2T} < S_T \\ -K_{2T}\dfrac{S_T - K_{1T}}{K_{1T} - K_{2T}}, & K_{2T} < K_{1T} < S_T \end{cases}$$

Together, this yields the approximation

$$x \approx \begin{cases} K_{1T}\left(1 - \varepsilon\dfrac{S_T - K_{2T}}{K_{2T} - K_{1T}}\right), & K_{1T} < K_{2T} < S_T \\ K_{2T}\left(1 - \varepsilon\dfrac{S_T - K_{1T}}{K_{1T} - K_{2T}}\right), & K_{2T} < K_{1T} < S_T \end{cases} \tag{74}$$

which has been used to construct the solution in Eq. (31).

For large S_T the term εS_T must not be neglected against K_{1T} and K_{2T} in the linear term of Eq. (71). Specifically, if $\varepsilon S_T \gg K_{1T} + K_{2T}$ the linear term becomes dominant so that balancing it with the $\mathcal{O}(1)$ part of the constant term yields the asymptotic form of the solution (cf. Eq. (29))

$$x \sim \frac{K_{1T}K_{2T}}{K_{1T} + K_{2T} + \varepsilon S_T}, S_T \gg \frac{K_{1T} + K_{2T}}{\varepsilon}.$$

A.2.2 Negative cooperativity

In the case of strong negative cooperativity ($c \ll b$) we rewrite Eq. (27) in the form

$$x^2 - (K_{1T} + K_{2T} - (1+\eta)S_T)x - \eta K_{1T}K_{2T} = 0 \tag{75}$$

where

$$\eta = \frac{c}{b-c} \ll 1.$$

Substituting the Ansatz

$$x = x_0 + \eta x_1 + \mathcal{O}\left(\eta^2\right)$$

into Eq. (75) yields

$$(x_0 - K_{1T} + K_{2T} - S_T)x_0 = 0 \tag{76}$$

and

$$2x_0x_1 - (K_{1T} + K_{2T} - S_T)x_1 + S_Tx_0 - K_{1T}K_{2T} = 0. \tag{77}$$

The non-negative solutions of Eq. (76) are given by

$$x_0^{(1)} = 0$$
$$x_0^{(2)} = K_{1T} + K_{2T} - S_T, S_T < K_{1T} + K_{2T}.$$

Substituting $x_0^{(i)}$ into Eq. (77) and solving for x_1 gives

$$x_1^{(1)} = \frac{K_{1T}K_{2T}}{S_T - (K_{1T} + K_{2T})}, S_T > K_{1T} + K_{2T}$$

$$x_1^{(2)} = -\left(S_T - \frac{K_{1T}K_{2T}}{K_{1T} + K_{2T} - S_T}\right), S_T < K_{1T} + K_{2T}.$$

Together, this yields the approximation (cf. Eq. (30))

$$x \approx \begin{cases} \eta\dfrac{K_{1T}K_{2T}}{S_T - (K_{1T} + K_{2T})}, & K_{1T} < S_T - K_{2T} \\ K_{1T} + K_{2T} - S_T, & K_{1T} > S_T - K_{2T} \end{cases} \tag{78}$$

which has been used to construct the solution in Eq. (32).

A.3 Stimulus response curve for substrate competition at large substrate concentration

The steady state for $[L1.R]$ is determined by the cubic equation in Eq. (35). To derive an approximate expression for the stimulus response curve in the limit $L1_T \gg (R_T - L2_T)/\varepsilon$ with $\varepsilon = K_{d2}/K_{d1} \ll 1$ we note that $[L1.R] \leq R_T$ remains bounded as $L1_T$ becomes large so that the cubic term can be neglected in that limit. Then, keeping only the dominant terms from the coefficients of the linear and the quadratic terms, the stimulus response curve is determined to leading order by

$$L_{1T}[L1.R]^2 - L1_T(R_T - L2_T - \varepsilon L1_T)[L1.R] + \varepsilon R_T L1_T^2 \approx 0$$

which agrees with Eq. (40).

Appendix B. Supplementary data

Supplementary data associated with this article can be found, in the online version, at https://doi.org/10.1016/j.biosystems.2017.10.012.

References

Adler, M., Mayo, A., Alon, U., 2014. Logarithmic and power law input–output relations in sensory systems with fold-change detection. PLoS Comput. Biol. 10, e1003781.

Alm, E., Huang, K., Arkin, A., 2006. The evolution of two-component systems in bacteria reveals different strategies for niche adaptation. PLoS Comput. Biol. 2, e143.

Amin, M., Kothamachu, V.B., Feliu, E., Scharf, B.E., Porter, S.L., Soyer, O.S., 2014. Phosphate sink containing two-component signaling systems as tunable threshold devices. PLoS Comput. Biol. 10, e1003890.

Babel, H., Bischofs, I.B., 2016. Molecular and cellular factors control signal transduction via switchable allosteric modulator proteins (SAMPs). BMC Syst. Biol. 10, 35.

Batchelor, E., Goulian, M., 2003. Robustness and the cycle of phosphorylation and dephosphorylation in a two-component regulatory system. Proc. Natl. Acad. Sci. U.S.A. 100, 691–696.

Blüthgen, N., Bruggeman, F.J., Legewie, S., Herzel, H., Westerhoff, H.V., Kholodenko, B.N., 2006. Effects of sequestration on signal transduction cascades. FEBS J. 273, 895–906.

Borghans, J.A.M., de Boer, R.J., Segel, L.A., 1996. Extending the quasi-steady state approximation by changing variables. Bull. Math. Biol. 58, 43–63.

Borisov, N.M., Markevich, N.I., Hoek, J.B., Kholodenko, B.N., 2005. Signaling through receptors and scaffolds: independent interactions reduce combinatorial complexity. Biophys. J. 89, 951–966.

Buchler, N.E., Louis, M., 2008. Molecular titration and ultrasensitivity in regulatory networks. J. Mol. Biol. 384, 1106–1119.

Capra, E.J., Perchuk, B.S., Skerker, J.M., Laub, M., 2012. Adaptive mutations that prevent crosstalk enable the expansion of paralogous signaling protein families. Cell 150, 222–232.

Chamnongpol, S., Cromie, M., Groisman, E.A., 2003. Mg^{2+} sensing by the Mg^{2+} sensor PhoQ of *Salmonella enterica*. J. Mol. Biol. 325, 795–807.

Cherfils, J., Zeghouf, M., 2013. Regulation of small GTPases by GEFs, GAPs, and GDIs. Physiol. Rev. 93, 269–309.

Ciliberto, A., Capuani, F., Tyson, J.J., 2007. Modeling networks of coupled enzymatic reactions using the total quasi-steady state approximation. PLoS Comput. Biol. 3, e45.

Conradi, C., Flockerzi, D., Raisch, J., Stelling, J., 2007. Subnetwork analysis reveals dynamic features of complex (bio)chemical networks. Proc. Natl. Acad. Sci. U.S.A. 104, 19175–19180.

Cornish-Bowden, A., 2004. Fundamentals of Enzyme Kinetics, 3rd ed. Portland Press, London.

Craciun, G., Tang, Y., Feinberg, M., 2006. Understanding bistability in complex enzyme-driven reaction networks. Proc. Natl. Acad. Sci. U.S.A. 103, 8697–8702.

Dasgupta, T., Croll, D.H., Owen, J.A., Van der Heiden, M.G., Locasale, J.W., Alon, U., Cantley, L.C., Gunawardena, J., 2014. A fundamental trade-off in covalent switching and its circumvention by enzyme bifunctionality in glucose homeostasis. J. Biol. Chem. 289, 13010–13025.

Dexter, J.P., Dasgupta, T., Gunawardena, J., 2015. Invariants reveal multiple forms of robustness in bifunctional enzyme systems. Integr. Biol. 7, 883–894.

Dexter, J.P., Gunawardena, J., 2013. Dimerization and bifunctionality confer robustness to the isocitrate dehydrogenase regulatory system in *Escherichia coli*. J. Biol. Chem. 288, 5770–5778.

Dubey, B.N., Lori, C., Ozaki, S., Fucile, G., Plaza-Menacho, I., Jenal, U., Schirmer, T., 2016. Cyclic di-GMP mediates a histidine kianse/phosphatase switch by noncovalent domain cross-linking. Sci. Adv. 2, e1600823.

Dye, B.T., Schulman, B.A., 2007. Structural mechanisms underlying posttranslational modification by ubiquitin-like proteins. Annu. Rev. Biophys. Biomol. Struct 36, 131–150.

Ehlert, F.J., 1988. Estimation of the affinities of allosteric ligands using radioligand binding and pharmacological null methods. Mol. Pharmacol. 33, 187–194.

Enserink, J.M., Kolodner, R.D., 2010. An overview of CDK1-controlled targets and processes. Cell Div. 5, 11.

Estrada, J., Wong, F., DePace, A., Gunawardena, J., 2016. Information integration and energy expenditure in gene regulation. Cell 166, 234–244.

Feliu, E., Knudsen, M., Andersen, L.N., Wiuf, C., 2012. An algebraic approach to signaling cascades with *n* layers. Bull. Math. Biol. 74, 45–72.

Ferrell Jr., J.E., 2002. Self-perpetuating states in signal transduction: positive feedback, double-negative feedback and bistability. Curr. Opin. Cell Biol. 14, 140–148.

Ferrell Jr., J.E., Ha, S.H., 2014. Ultrasensitivity. Part II: multisite phosphorylation, stoichiometric inhibitors, and positive feedback. Trends Biochem. Sci. 39, 556–569.

Fisher, S.L., Kim, S.K., Wanner, B.L., Walsh, C.T., 1996. Kinetic comparison of the specificity of the vancomycin kinase VanS for two response regulators, VanR and PhoB. Biochemistry 35, 4732–4740.

Gao, R., Stock, A.M., 2013. Probing kinase and phosphatase activities of two-component systems *in vivo* with concentration-dependent phosphorylation profiling. Proc. Natl. Acad. Sci. U.S.A. 110, 672–677.

Garcia, E., Rhee, S.G., 1983. Cascade control of *Escherichia coli* glutamine synthetase. J. Biol. Chem. 258, 2246–2253.

Geontoro, L., Shoval, O., Kirschner, M.W., Alon, U., 2009. The incoherent feedforward loop can provide fold-change detection in gene regulation. Mol. Cell 36, 894–899.

Goldbeter, A., Koshland Jr., D.E., 1981. An amplified sensitivity arising from covalent modification in biological systems. Proc. Natl. Acad. Sci. U.S.A. 78, 6840–6844.

Gomez-Uribe, C., Verghese, G.C., Mirny, L.A., 2007. Operating regimes of signaling cycles: statics, dynamics and noise filtering. PLoS Comput. Biol. 3, e246.

Goody, R.S., Hofmann-Goody, W., 2002. Exchange factors, effectors, GAPs and motor proteins: common thermodynamic and kinetic principles for different functions. Eur. Biophys. J 31, 268–274.

Goryachev, A.B., Pokhilko, A.V., 2006. Computational model explains high activity and rapid cycling of Rho GTPases within protein complexes. PLoS Comput. Biol. 2, e172.

Goulian, M., 2010. Two-component signaling circuit structure and properties. Curr. Opin. Microbiol. 13, 184–189.

Grimshaw, C.E., Huang, S., Hanstein, C.G., Strauch, M.A., Burbulys, D., Wang, L., Hoch, J.A., Whiteley, J.M., 1998. Synergistic kinetic interactions between components of the phosphorelay controlling sporulation in *Bacillus subtilis*. Biochemistry 37, 1365–1375.

Groban, E.S., Clarke, E.J., Salis, H.M., Miller, S.M., Voigt, C.A., 2009. Kinetic buffering of cross talk between bacterial two-component sensors. J. Mol. Biol. 390, 380–393.

Gu, C., Nguyen, H.-N., Hofer, A., Jessen, H.J., Dai, X., Wang, H., Shears, S.B., 2017. The significance of the bifunctional kinase/phosphatase activities of PPIP5Ks for coupling inositol pyrophosphate cell-signaling to cellular phosphate homeostasis. J. Biol. Chem. 292, 4544–4555.

Gunawardena, J., 2005. Multisite protein phosphorylation makes a good threshold but can be a poor switch. Proc. Natl. Acad. Sci. U.S.A. 102, 14617–14622.

Ha, S.H., Ferrell Jr., J.E., 2016. Thresholds and ultrasensitivity from negative cooperativity. Science 352, 990–993.

Ha, S.H., Kim, S.Y., Ferrell Jr., J.E., 2016. The prozone effect accounts for the paradoxical function of the Cdk-binding protein Suc1/Cks. Cell Rep. 14, 1408–1421.

Hart, Y., Madar, D., Yuan, J., Bren, A., Mayo, A.E., Rabinowitz, J.D., Alon, U., 2011a. Robust control of nitrogen assimilation by a bifunctional enzyme in *E. coli*. Mol. Cell 41, 117–127.

Hart, Y., Mayo, A.E., Milo, R., Alon, U., 2011b. Robust control of PEP formation rate in the carbon fixation pathway of c_4 plants by a bifunctional enzyme. BMC Syst. Biol. 5, 171.

Heermann, R., Jung, K., 2010. The complexity of the 'simple' two-component system KdpD/KdpE in *Escherichia coli*. FEMS Microbiol. Lett. 304, 97–106.

Heinrich, R., Neel, B.G., Rapoport, T.A., 2002. Mathematical models of protein kinase signal transduction. Mol. Cell 9, 957–970.

Igoshin, O.A., Alves, R., Savageau, M.A., 2008. Hysteretic and graded responses in bacterial two-component signal transduction. Mol. Microbiol. 68, 1196–1215.

Jiang, P., Ninfa, A.J., 1999. Regulator of autophosphorylation of *Escherichia coli* nitrogen regulator II by the PII signal transduction protein. J. Bacteriol. 181, 1906–1911.

Jiang, P., Ventura, A.C., Ninfa, A.J., 2012. Characterization of the reconstituted UTase/UR-PII-NRII-NRI bicyclic signal transduction system that controls the transcription of nitrogen-regulated (Ntr) genes in *Escherichia coli*. Biochemistry 51, 9045–9057.

Kim, S.Y., Ferrell Jr., J.E., 2007. Substrate competition as a source of ultrasensitivity in the inactivation of Wee1. Cell 128, 1133–1145.

Kim, Y., Andreu, M.J., Lim, B., Chung, K., Terayama, M., Jiménez, G., Berg, C.A., Lu, H., Shvartsman, S.Y., 2011. Gene regulation by MAPK substrate competition. Dev. Cell 20, 880–887.

Kim, Y., Coppey, M., Grossman, R., Ajuria, L., Jiménez, G., Paroush, Z., Shvartsman, S.Y., 2010. MAPK substrate competition integrates patterning signals in the *Drosophila* embryo. Curr. Biol. 20, 446–451.

Krell, T., Lacal, J., Busch, A., Silva-Jiménez, H., Guazzaroni, M.-E., Ramos, J.L., 2010. Bacterial sensor kinases: diversity in the recognition of environmental signals. Annu. Rev. Microbiol. 64, 539–559.

Kremling, A., Heermann, R., Centler, F., Jung, K., Gilles, E.D., 2004. Analysis of two-component signal transduction by mathematical modeling using the *KdpD/KdpE* system of *Escherichia coli*. Biosystems 78, 23–37.

Kurland, I.J., Pilkis, S.J., 1995. Covalent control of 6-phosphofructo-2-kinase/fructose-2,6-bisphosphatase: insights into autoregulation of a bifunctional enzyme. Protein Sci. 4, 1023–1037.

Kuznetsov, Y.A., 1998. Elements of Applied Bifurcatuion Theory. Springer Verlag, New York.

LaPorte, D.C., Koshland Jr., D.E., 1982. A protein with kinase and phosphatase activities involved in regulation of tricarboxylic acid cycle. Nature 300, 458–460.

LaPorte, D.C., Koshland Jr., D.E., 1983. Phosphorylation of isocitrate dehydrogenase as a demonstration of enhanced sensitivity in covalent regulation. Nature 305, 286–290.

LaPorte, D.C., Thorsness, P.E., Koshland Jr., D.E., 1985. Compensatory phosphorylation of isocitrate dehydrogenase: a mechanism for adaption to the intracellular environment. J. Biol. Chem. 260, 10563–10568.

Laub, M.T., Goulian, M., 2007. Specificity in two-component signal transduction pathways. Annu. Rev. Genet. 41, 121–145.

Legewie, S., Herzel, H., Westerhoff, H.V., Blüthgen, N., 2008. Recurrent design patterns in the feedback regulation of the mammalian signalling network. Mol. Syst. Biol. 4, 190.

Levine, E., Zhang, Z., Kuhlman, T., Hwa, T., 2007. Quantitative characteristics of gene regulation by small RNA. PLoS Biol. 5, e229.

Levine, J.H., Lin, Y., Elowitz, M.B., 2013. Functional roles of pulsing in genetic circuits. Science 342, 1193–1200.

Lydeard, J.R., Schuman, B.A., Harper, J.W., 2013. Building an remodelling cullin-RING E3 ubiquitin ligases. EMBO Rep. 14, 1050–1061.

Markevich, N.I., Hoek, J.B., Kholodenko, B.N., 2004. Signaling switches and bistability arising from multisite phosphorylation in protein kinase cascades. J. Cell Biol. 164, 353–359.

Masia, M.D., Garcia-Moreno, M., Garcia-Sevilla, F., Escribano, J., Molina-Alarcon, M., Amo-Saus, M.L., Ortiz-Ruiz, C.V., Varon, R., 2016. A novel transient phase kinetic analysis of the fractional modification of monocyclic enzyme cascades. J. Math. Chem. 54, 1952–1972.

Milo, R., Shen-Orr, S., Itzkovitz, S., Kashtan, N., Chklovskii, D., Alon, U., 2002. Network motifs: simple building blocks of complex networks. Science 298, 824–827.

Mitarai, N., Andersson, A.M.C., Krishna, S., Semsey, S., Sneppen, K., 2007. Efficient degradation and expression prioritization with small RNAs. Phys. Biol. 4, 164–171.

Miyashiro, T., Goulian, M., 2008. High stimulus unmasks positive feedback in autoregulated bacterial signaling circuit. Proc. Natl. Acad. Sci. U.S.A. 105, 17457–17462.

Mukherji, S., Ebert, M.S., Zheng, G.X.Y., Tsang, J.S., Sharp, P.A., van Oudenaarden, A., 2011. MicroRNAs can generate thresholds in target gene expression. Nat. Genet. 43, 854–859.

Ninfa, A.J., Jiang, P., Atkinson, M.R., Peliska, J.A., 2000. Integration of antagonistic signals in the regulation of nitrogen assimilation in *Escherichia coli*. Curr. Top. Cell. Regul. 36, 31–75.

Novak, B., Tyson, J.J., 2008. Design principles of biochemical oscillators. Nat. Rev. Mol. Cell Biol. 9, 981–991.

Olsman, N., Geontoro, L., 2016. Allosteric proteins as logarithmic sensors. Proc. Natl. Acad. Sci. U.S.A. 113, 4423–4430.
Ortega, F., Acerenza, L., Westerhoff, H.V., Mas, F., Cascante, M., 2002. Product dependence and bifunctionality compromise the ultrasensitivity of signal transduction cascades. Proc. Natl. Acad. Sci. U.S.A. 99, 1170–1175.
Pedersen, M.G., Bersani, A.M., Bersami, E., Cortese, G., 2010. The total quasi-steady state approximation for complex enzyme reactions. J. Math. Biol. 60, 267–283.
Pedersen, M.G., Bersani, A.M., Bersani, E., 2007. The total quasi-steady state approximation for fully competitive enzyme reactions. Bull. Math. Biol. 69, 433–457.
Petroski, M.J., Deshaies, R.J., 2005. Function and regulation of cullin-ring ubiquitin ligases. Nat. Rev. Mol. Cell Biol. 6, 9–20.
Podgornaia, A.I., Laub, M.T., 2013. Determinants of specificity in two-component signal transduction. Curr. Opin. Microbiol. 16, 156–162.
Rosenfeld, N., Young, J.W., Alon, U., Swain, P.S., Elowitz, M.B., 2007. Accurate prediction of gene feedback circuit behavior from component properties. Mol. Syst. Biol. 3, 143.
Rowland, M.A., Deeds, E.J., 2014. Crosstalk and the evolution of specificity in two-component signaling. Proc. Natl. Acad. Sci. U.S.A. 111, 5550–5555.
Rowland, M.A., Fontana, W., Deeds, E.J., 2012. Crosstalk and competition in signaling networks. Biophys. J. 103, 2389–2398.
Russo, F.D., Silhavy, T.J., 1993. The essential tension: opposed reactions in bacterial two-component regulatory systems. Trends Microbiol. 1, 306–310.
Salazar, C., Höfer, T., 2009. Multisite protein phosphorylation – from molecular mechanisms to kinetic models. FEBS J. 276, 3177–3198.
Sasagawa, S., Ozaki, Y., Fujita, K., Kuroda, S., 2005. Prediction and validation of the distinct dynamics of transient and sustained ERK activation. Nat. Cell Biol. 7, 365–373.
Sauro, H.M., Kholodenko, B.N., 2004. Quantitative analysis of signaling networks. Prog. Biophys. Mol. Biol. 86, 5–43.
Schnell, S., Maini, P.K., 2000. Enzyme kinetics at high enzyme concentrations. Bull. Math. Biol. 62, 483–499.
Segel, L.A., Slemrod, M., 1989. The quasi-steady state assumption: a case study in perturbation. SIAM Rev. 31, 446–477.
Shin, D., Lee, E.J., Huang, H., Groisman, E.A., 2006. A positive feedback loop promotes surge that jump-starts *Salmonella* virulence circuit. Science 314, 1607–1609.
Shinar, G., Feinberg, M., 2010. Structural sources of robustness in biochemical reaction networks. Science 327, 1389–1391.
Shinar, G., Milo, R., Martinez, M.R., Alon, U., 2007. Input–output robustness in simple bacterial signaling systems. Proc. Natl. Acad. Sci. U.S.A. 104, 19931–19935.
Shinar, G., Rabinowitz, J.D., Alon, U., 2009. Robustness in glyoxylate bypass regulation. PLoS Comput. Biol. 5, e1000297.
Siryaporn, A., Goulian, M., 2008. Cross-talk suppression between the CpxA-CpxR and EnvZ-OmpR two-component systems in *E. coli*. Mol. Microbiol. 70, 494–506.
Siryaporn, A., Perchuk, B.S., Laub, M.T., Goulian, M., 2010. Evolving a robust signal transduction pathway from weak cross-talk. Mol. Syst. Biol. 6, 452.
Skerker, J.M., Prasol, M.S., Perchuk, B.S., Biondi, E.G., Laub, M.T., 2005. Two-component signal transduction pathways regulating growth ad cell cycle progression in a bacterium: a system-level analysis. PLoS Biol. 3, e334.
Sontag, E.D., 2017. Dynamic compensation, parameter identifiability, and equivariances. PLoS Comput. Biol. 13, e1005447.
Sourjik, V., 2004. Receptor clustering and signal processing in *E. coli* chemotaxis. Trends Microbiol. 12, 569–576.
Stewart, R.C., 2010. Protein histidine kinases: assembly of active sites and their regulation in signaling pathways. Curr. Opin. Microbiol. 13, 133–141.
Stock, A.M., Robinson, V.L., Goudreau, P.N., 2000. Two-component signal transduction. Annu. Rev. Biochem. 69, 183–215.
Straube, R., 2012. Comment on 'load-induced modulation of signal transduction networks': Reconciling ultrasensitivity with bifunctionality? Sci. Signal. 5, lc1.
Straube, R., 2013. Sensitivity and robustness in covalent modification cycles with a bifunctional converter enzyme. Biophys. J. 105, 1925–1933.
Straube, R., 2014. Reciprocal regulation as a source of ultrasensitivity in two-component systems with a bifunctional sensor kinase. PLoS Comput. Biol. 10, e1003614.
Straube, R., 2015. Analysis of substrate competition in regulatory network motifs: stimulus-response curves, thresholds and ultrasensitivity. J. Theor. Biol. 380, 74–82.
Straube, R., 2017. Operating regimes of covalent modification cycles at high enzyme concentrations. J. Theor. Biol. 431, 39–48.
Straube, R., Conradi, C., 2013. Reciprocal enzyme regulation as a source of bistability in covalent modification cycles. J. Theor. Biol. 330, 56–74.
Straube, R., Flockerzi, D., Wolf, D.A., 2017. Trade-off and flexibility in the dynamic regulation of the cullin-RING ubiquitin ligase repertoire. PLoS Comput. Biol. 10, e172.
Thomson, M., Gunawardena, J., 2009. Unlimited multistability in multisite phopshorylation systems. Nature 460, 274–277.
Thurley, K., Skupin, A., Thul, R., Falcke, M., 2012. Fundamental properties of Ca^{2+} signals. Biochim. Biophys. Acta 1820, 1185–1194.
Tindall, M.J., Porter, S.L., Maini, P.K., Armitage, J.P., 2013. Modeling chemotaxis reveals the role of reversed phosphotransfer and bi-functional kinase-phosphatase. PLoS Comput. Biol. 6, e1000896.
Tiwari, A., Ray, J.C.J., Narula, J., Igoshin, O.A., 2011. Bistable responses in bacterial genetic networks: designs and dynamical consequences. Math. Biosci. 231, 76–89.
Tzafriri, A.R., 2003. Michaelis-Menten kinetics at high enzyme concentrations. Bull. Math. Biol. 65, 1111–1129.
Tzafriri, A.R., Edelman, E.R., 2004. The total quasi-steady state approximation is valid for reversible enzyme kinetics. J. Theor. Biol. 226, 303–313.
Ubersax, J.A., Woodbury, E.L., Quang, P.N., Paraz, M., Blethrow, J.D., Shah, K., Shokat, K.M., Morgan, D.O., 2003. Targets of the cyclin-dependent kinase cdk1. Nature 425, 859–864.
Ventura, A.C., Jiang, P., Van Wassenhove, L., Del Vecchio, D., Merajver, S.D., Ninfa, A.J., 2010. Signaling properties of a covalent modification cycle are altered by a downstream target. Proc. Natl. Acad. Sci. U.S.A. 107, 10032–10037.
Wei, K., Moinat, M., Maarleveld, T.R., Bruggeman, F.J., 2014. Stochastic simulation of procaryotic two-component signalling indicates stochasticity-induced active-state locking and growth-rate dependent bistability. Mol. Biosyst 10, 2338–2346.
Witzel, F., Maddison, L., Blüthgen, N., 2012. How scaffolds shape MAPK signaling: what we know and opportunities for systems approaches. Front. Physiol. 3, 475.
Zheng, J., Jia, Z., 2010. Structure of the bifunctional isocitrate dehydrogenase kinase/phosphatase. Nature 465, 961–965.